

Pion-Nucleon Scattering in a New Approach to Chiral Perturbation Theory

Paul J. Ellis and Hua-Bin Tang

School of Physics and Astronomy, University of Minnesota, Minneapolis, MN 55455.

(September 15, 1996)

Abstract

We study pion-nucleon scattering with a chiral lagrangian of pions, nucleons, and Δ -isobars. The scattering amplitude is evaluated to one-loop Q^3 order, where Q is a generic small momentum, using a new approach which is equivalent to heavy baryon chiral perturbation theory. We obtain a good fit to the experimental phase shifts for pion center-of-mass kinetic energies up to 100 MeV. A sigma term greater than 45 MeV is favored, but the value is not well determined.

PACS number(s): 21.30.+y, 21.60.Jz, 21.65.+f

I. INTRODUCTION

The pion and the nucleon play a central role in low-energy physics and there is a wealth of scattering data which allow us to test the application of effective Lagrangians. Several relativistic phenomenological models [1-6] exist, which provide reasonably good fits to the experimental πN phase shifts. In these models either the Bethe-Salpeter equation is solved approximately or the K -matrix method is used to unitarize the tree amplitudes. Such models, however, do not offer a systematic approximation scheme.

Chiral perturbation theory (ChPT) [7,8] is a more attractive approach because it not only embodies chiral symmetry, which is fundamental to low-energy physics, but it also offers a systematic expansion in powers of the momentum. Further it ensures unitarity order by order. Gasser and Leutwyler [8] have shown that ChPT works nicely for mesons; however, the power counting fails when baryons are introduced [9]. The power counting can be restored in heavy baryon chiral perturbation theory (HBChPT) [10] where the heavy components of the baryon fields are integrated out. Here we shall adopt a different approach [11] which effectively removes the heavy fields after constructing the Feynman diagrams. This new approach preserves the power counting and gives results in agreement with HBChPT, at least to the order considered.

Peccei [12] was the first to use a chiral lagrangian to calculate the πN scattering lengths near threshold. Calculations with the more modern approach of HBChPT are discussed by Bernard et al. in a review [13] and in Refs. [14,15]. Particularly interesting is the recent calculation by Mojzis [16] of the full amplitude to $O(Q^3)$, with Q a generic small momentum scale. Mojzis employs just pion and nucleon fields. Since there are a number of unknown parameters, scattering lengths and effective ranges alone are not a stringent test of the approach. We mention that Datta and Pakvasa [17] have recently used the results of Mojzis to discuss low-energy scattering. However a fit to the phase shifts out to center-of-mass (cm.) energies in the resonance region is desirable. This requires explicit consideration of the field itself, along with the pion and nucleon fields. Here we shall carry out this

program by evaluating all diagrams up to one-loop Q^3 order.

The organization of this paper is as follows. In Sec. II we write down our effective lagrangian and establish our notation. In Sec. III we describe our method of separating out the soft contributions, which need to be calculated, from the hard contributions, which are subsumed in the parameters. Fermion loops and the implications for power counting are also discussed here. The formalism for NN scattering is given in Sec. IV, with a listing of the expressions for the loop diagrams relegated to the Appendix. The calculated phase shifts are compared with the data in Sec. V, where we also discuss the effective NN and NN couplings as well as the pion-nucleon σ term. Our conclusions are given in Sec. VI.

II. EFFECTIVE LAGRANGIAN

Before writing down an effective chiral lagrangian we need to define our notation, much of which is fairly standard. The Goldstone pion fields $\pi^a(x)$, with $a = 1, 2, 3$, form an isotriplet that can be written in terms of an $SU(2)$ matrix:

$$U(x) = \exp(2i \pi^a(x) \tau^a / f) ; \quad (1)$$

where $f \approx 93 \text{ MeV}$ is the pion decay constant and the pion field is compactly written as $\pi(x) = \frac{1}{2} \tau^a \pi^a(x)$, with τ^a being the Pauli matrices. The matrix U is the standard exponential representation and the "square root" representation in terms of π is particularly convenient for including heavy fields in the chiral lagrangian. The isodoublet nucleon field is represented by a column matrix

$$N = \begin{pmatrix} p \\ n \end{pmatrix} = \begin{pmatrix} p \\ n \end{pmatrix} ; \quad (2)$$

where p and n are the proton and neutron fields respectively. The Δ is a spin- $\frac{3}{2}$ and isospin- $\frac{3}{2}$ particle represented by an isosquadruplet field:

$$= \begin{pmatrix} 0 & 1 \\ \frac{1}{\sqrt{2}} & 0 \end{pmatrix} = \begin{pmatrix} \frac{1}{\sqrt{2}} & 0 \\ 0 & 1 \end{pmatrix} \quad (3)$$

It is convenient to introduce an isovector field $\mathbf{A} = T$ in terms of the standard 2×4 isospin $\frac{3}{2}$ to $\frac{1}{2}$ transition matrix:

$$h \frac{1}{2} \tau \cdot T \frac{3}{2} \tau = i \quad h \frac{1}{2} \tau \cdot T \frac{3}{2} \tau = i e \quad ; \quad (4)$$

where the isospin spherical unit vectors are $e_0 = e_z$ and $e_{\pm 1} = \frac{1}{\sqrt{2}}(e_x \pm i e_y) = \frac{1}{\sqrt{2}}$. Explicitly, the components are

$$h \frac{1}{2} \tau \cdot T \frac{3}{2} \tau = i \quad h \frac{1}{2} \tau \cdot T \frac{3}{2} \tau = i e \quad ; \quad (5)$$

$$h \frac{1}{2} \tau \cdot T \frac{3}{2} \tau = i \quad h \frac{1}{2} \tau \cdot T \frac{3}{2} \tau = i e \quad ; \quad (6)$$

$$h \frac{1}{2} \tau \cdot T \frac{3}{2} \tau = i \quad h \frac{1}{2} \tau \cdot T \frac{3}{2} \tau = i e \quad ; \quad (7)$$

Following Callan et al. [18] we define a nonlinear realization of the chiral group $SU(2)_L$ $SU(2)_R$ such that, for arbitrary global matrices $L \in SU(2)_L$ and $R \in SU(2)_R$, we have the mapping

$$L \quad R : \quad (\quad ; N \quad) \quad ! \quad (\quad ; N \quad ; \quad) \quad ; \quad (8)$$

where

$$h^0(x) = L \quad (x) h^y(x) = h(x) \quad (x) R^y \quad ; \quad (9)$$

$$N^0(x) = h(x) N \quad (x) \quad ; \quad (10)$$

$$h^0(x) = \frac{1}{2} h \text{tr}(h \quad h^y \quad) \quad (x) \quad : \quad (11)$$

As usual, the matrix U transforms as $U^0(x) = L U(x) R^Y$. The second equality in Eq. (9) defines $h(x)$ implicitly as a function of L, R , and the local pion fields: $h(x) = h(x; L; R)$. The pseudoscalar nature of the pion field implies $h(x) \in SU(2)_V$, with $SU(2)_V$ the unbroken vector subgroup of $SU(2)_L \times SU(2)_R$. The nucleon transforms linearly under $SU(2)_V$ as an isodoublet. While the isodoublet components of the isovector transform linearly in the same way as the nucleon field, the isovector itself is further rotated by the $O(3)$ transformation $\frac{1}{2}\text{tr}(h^\dagger h^Y)$.

Interaction terms invariant under the nonlinear chiral transformation may be conveniently constructed in terms of an axial vector field $a(x)$ and a polar vector field $v(x)$ defined as

$$a = \frac{i}{2} (\gamma^Y \partial_\mu - \partial_\mu \gamma^Y) = a^Y = \frac{1}{2} a = \frac{1}{f} \partial_\mu \left[\frac{1}{3f^3} [\gamma^Y; \partial_\mu] + \dots \right]; \quad (12)$$

$$v = \frac{i}{2} (\gamma^Y \partial_\mu + \partial_\mu \gamma^Y) = v^Y = \frac{1}{2} v = \frac{i}{2f^2} \left[1 - \frac{1}{3f^2} [\gamma^Y; \partial_\mu] + \dots \right]; \quad (13)$$

both of which contain one derivative. The polar vector field transforms inhomogeneously and the axial vector field transforms homogeneously:

$$v^0 = h v h^Y - i h \partial h^Y; \quad (14)$$

$$a^0 = h a h^Y; \quad (15)$$

To maintain chiral invariance, instead of an ordinary derivative ∂ , one uses a covariant derivative D on the nucleon and pion fields. These are defined by

$$D N = \partial N + i v N; \quad (16)$$

$$D = \partial + i v \quad : \quad (17)$$

We also use the following definitions involving two and three derivatives on the pion field

$$v = \partial v - \partial v + i[v; v] = i[a; a]; \quad (18)$$

$$D a = \partial a + i[v; a]; \quad (19)$$

$$D v = \partial v + i[v; v]; \quad (20)$$

all of which transform homogeneously in the same way as a in Eq. (15).

To write a general effective lagrangian, we need an organizational scheme for the interaction terms. We organize the lagrangian in increasing powers of the fields and their derivatives. Specifically, as in Refs. [6,19], we assign to each interaction term a size of order Q with

$$= d + \frac{n}{2} ; \quad (21)$$

where d is the number of derivatives on the pion field or pion mass (m) factors, and n is the number of fermion fields in the interaction term. That is a characteristic of the interaction term is suggested by Weinberg's power counting [20], which we discuss in Sec. III below. Derivatives on the nucleon fields are not counted in d because they will generally be associated with the nucleon mass and not with the small momentum Q . In fact, as Krause [21] has argued, it is D/M that is of $O(Q^1)$. Krause also counts ψ to be of $O(Q^0)$ and a single factor of ψ to be of $O(Q^1)$. We adopt this counting for organizing the lagrangian, although we have argued [6] that counting a single ψ factor to be of $O(Q^1)$ is not precise. Our scheme allows a uniform organization of the pion self-interaction terms and those involving the heavy fermions. It differs from the "standard labelling" of Gasser, Sainio and Svarc [9] where the number of fermion fields is not included.

Taking into account chiral symmetry, Lorentz invariance, and parity conservation, we may write the lagrangian through quartic order (4) as the sum of the order Q^2 , Q^3 , and Q^4 parts:

$$L = L_2 + L_3 + L_4 + L ; \quad (22)$$

where L represents the counterterms, which can also be organized in powers of Q . We will adopt the counterterm method of renormalization, so we start with the physical masses and couplings and add the necessary counterterms. For simplicity, in this first investigation we will not explicitly identify the finite and divergent pieces of the various counterterms. The order Q^2 part of the lagrangian is

$$L_2 = \bar{N} (\not{D} + g_A \gamma_5 a \cdot M) N + \frac{1}{4} f^2 \text{tr} (\partial_\mu U^\dagger \partial^\mu U) + \frac{1}{4} m^2 f^2 \text{tr} (U + U^\dagger - 2) \\ + \bar{a}_{ab} \gamma^a \gamma^b + h_A \bar{a} \cdot N + \bar{N} a + \bar{h}_A \bar{a} \cdot \gamma_5 a \cdot a ; \quad (23)$$

where the isospin indices $a, b = 1, 2$; and 3, the trace is taken over the isospin matrices, and the kernel tensor in the kinetic-energy term is

$$= (\not{D} - M) g + i(\not{D} + D) (\not{D} + M) ; \quad (24)$$

suppressing isospin indices. Here we have chosen the standard parameter $A = 1$, because it can be modified by redefinition of the field with no physical consequences [22]. In the NN interaction of Eq. (23) we have chosen the standard σ -shell Z parameter to have the convenient value of $\frac{1}{2}$. The value of Z has no physical significance since modifications can be absorbed in the other parameters in the lagrangian [23]. Similarly we simplify the πNN interaction by choosing the σ -shell parameters defined in Ref. [23] to be $Z_2 = \frac{1}{2}$ and $Z_3 = 0$.

With the notation

$$\not{D} = D \quad (\partial_\mu \gamma^\mu) ; \quad (25)$$

we may write the order Q^3 and Q^4 parts of L as follows:

$$L_3 = \frac{1}{M} \bar{N} N \text{tr} (\partial_\mu U^\dagger \partial^\mu U) - \frac{1}{M} \bar{N} \not{v} \cdot N \\ + \frac{1}{2M^2} \bar{N} \not{D} \not{D} N \text{tr} (a \cdot a) + \frac{2}{M} m^2 \bar{N} N \text{tr} (U + U^\dagger - 2) + \quad ; \quad (26)$$

$$L_4 = \frac{1}{M} m^2 \bar{N} \gamma_5 (U - U^\dagger) N + \frac{2}{M^2} \bar{N} \not{D} \not{v} \cdot N \\ + \frac{3}{M^2} m^2 \bar{N} \not{a} \cdot U - U^\dagger N + \frac{4}{2M^3} \bar{N} \not{D} \not{D} N \text{tr} (a \cdot D \cdot a) \\ + \frac{5}{16M^4} \bar{N} \not{f}_D \not{D} \not{g}^a N \text{tr} (\gamma^a \not{D} \gamma^a ; a) \\ + \frac{6}{M^2} m^2 \text{tr} [\partial_\mu (U - U^\dagger) N + \bar{N} \partial_\mu (U - U^\dagger)]^0 + \quad : \quad (27)$$

In Eqs. (26) and (27) the ellipsis represents terms that do not contribute to the NN scattering amplitude. For example, the ellipsis in L_4 includes the usual pion self-interaction terms with

four derivatives. The m^2 factors in L_4 are introduced to correctly count the order of the symmetry breaking terms. However, it appears that counterterms of the above form with m^2 replaced by μ^2 are needed even in the chiral limit ($m = 0$). Here $\mu = M - M$ is the Σ -nucleon mass difference. We have applied naive dimensional analysis [19,24] to the terms in Eqs. (26) and (27) so as to expose the dimensional factors. As a result, we expect the parameters to be of order unity.

Using the pion and nucleon equations of motion [20,25,26], we have also simplified the contact terms listed in Ref. [9]. For example, we reduce the $O(Q^3)$ term $\bar{N} \not{D} \not{D} N \text{tr}(a a)$ to the sum of the $O(Q^3)$ term, the $O(Q^4)$ term, and higher-order terms which we omit. As a result we have the minimum number of independent terms contributing to the ΣN scattering amplitude up to $O(Q^3)$. Note that the isoscalar-scalar and isovector-vector fields given in Ref. [19] have been integrated out. Their effects show up in the contact terms α_1 ; α_2 and α_3 . For example, in terms of the ΣN coupling (g_Σ) and the $\Sigma N N$ coupling (g_Σ), the rho gives a contribution to the α_2 parameter of $2g_\Sigma g_\Sigma M^2 f^2 = m^4$.

III. CHIRAL PERTURBATION THEORY WITH BARYONS

A. Hard and Soft Contributions

Given the effective lagrangian, one can derive the Feynman rules and carry out perturbative calculations of physical quantities in the standard way. However, as shown by Gasser, Sainio and Svarc [9], the loop expansion no longer corresponds directly to the momentum expansion when we have heavy fermions. One way to overcome this difficulty is HBChPT [10], where the heavy components of the fermion fields are integrated out so that their effects on physical quantities only show up in the parameters of the lagrangian. Alternatively one can construct an explicitly nonrelativistic lagrangian [20].

We propose a different procedure here which involves manipulating the Feynman diagrams themselves (see also the recent discussion of Gasser [27]). First we obtain the Feynman

rules in the standard way. Then we separate the loop contributions into those from soft and hard momenta. We keep the soft contributions explicitly. These will have both real and imaginary parts in general, the latter being needed to maintain unitarity order by order. As for the hard contributions, we implicitly absorb them into the coefficients of the Lagrangian. As we will see this procedure preserves a systematic power counting scheme.

Specifically, we represent the hard momentum scale by the nucleon mass M . Other quantities of this order include the mass M and the factor $4f$ with 4 coming from a loop integral [28]. The soft momentum scale is denoted by Q , where $Q \ll M$. Quantities of this order are the pion mass m , the pion momentum, and the mass splitting between the nucleon and the Δ -isobar. Also, as in HBC hPT, we are interested in applications where the three-momenta of the external nucleons are of order Q .

For the present we consider any loop diagram without fermion loops: we shall consider diagrams with fermion loops later. We obtain the unrenormalized soft part of the diagram by applying the following rules to the loop integral:

1. Take the loop momenta of the pion lines to be of order Q .
2. Make a covariant $Q \ll M$ expansion of the integrand.
3. Exchange the order of the integration and summation of the power series.

Rule 1 ensures that the exchanged pions have soft momenta. As a result internal baryon lines will be nearly on shell throughout the diagram. Rule 2 implies that a covariant expansion of the baryon propagators in the integrand is made, which maintains the Lorentz invariance of the soft part. In Rule 3 the exchange of the order of integration and summation changes the result in general. Indeed the purpose of this maneuver is to remove the poles in the baryon propagators at hard loop momenta of order M . Clearly this is achieved because after application of Rule 2 the only poles in individual terms of the series are located in the soft momentum region of $O(Q)$. Of course the soft part obtained from our rules still contains ultraviolet divergences in the form of poles at $d = 4$ in dimensional regularization.

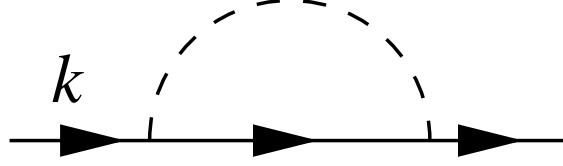


FIG .1. A one-loop nucleon self-energy diagram . The dashed line represents a pion propagator and the solid line a nucleon propagator.

We remove these divergences with the standard method of renormalization . Formally, if we denote the original integral by I , the unrenormalized soft part by $\hat{S}I$ and the renormalization operator by \hat{R} , the renormalized soft part is $\hat{R}\hat{S}I$. This is the physical loop contribution . As discussed in the next section, the soft loop contributions allow for a systematic power counting.

As for the part of the original integral I that is discarded, namely $I - \hat{R}\hat{S}I$, we call it the hard part. This hard part contains contributions from poles of the integrand at hard momenta . Thus, we should be able to absorb this part into the coefficients of the lagrangian . As Lepage [29] has argued from the uncertainty principle, large momenta correspond to short distances that are tiny compared with the wavelengths of the external particles, so the interactions must be local.

At this stage a concrete example is useful. Thus, we evaluate the nucleon self-energy diagram shown in Fig.1. From standard Feynman rules we obtain the self-energy:

$$\Sigma_N(k) = \frac{3g_A^2}{4f^2} i^{-4-d} \int \frac{d^d \ell}{(2\pi)^d} \frac{\gamma_5 G(k+\ell) \gamma_5}{\ell^2 - m^2 + i\epsilon}; \quad (28)$$

where the free nucleon propagator

$$G(k) = \frac{1}{\not{k} - M + i\epsilon}; \quad (29)$$

and ϵ is the scale of dimensional regularization. We obtain the soft part of Σ_N by first making a covariant $Q \rightarrow M$ expansion of the integrand, while taking the pion momentum ℓ to be soft. Since we assume k to be nearly on shell, we can make a covariant expansion of the nucleon propagator as

$$G(k + \ell) = \frac{1}{2k^2 + 2k^2 M^2 + i} (\ell + M) + \gamma \frac{\ell^2 (\ell + M)}{2k^2 + 2k^2 M^2 + i} + \dots : \quad (30)$$

Here the contribution arising from first term in the square brackets is of order Q^{-1} , while that due to the second and third terms is of order Q^{-1} ($Q=M$). Subsequent terms will involve higher powers of $Q=M$. The precise way this expansion is carried out has to be tailored to the case at hand. For example, in N scattering we have $k = (p + q)$ where $p^2 = M^2$ and $q^2 = m^2$. Then we may let $k \rightarrow p$ and $\ell \rightarrow (\ell + q)$ in Eq. (30).

Exchanging the order of the summation and integration in Eqs. (28) and (30) then yields the soft part:

$$\hat{S}_N(k) = \frac{3g_A^2}{4f^2} i^{4-d} \int \frac{d^d \ell}{(2\pi)^d} \frac{(2k - \ell) \gamma (\ell + M) \ell}{(\ell^2 - m^2 + i)(2k^2 - \ell^2 + 2k^2 M^2 + i)} + \dots : \quad (31)$$

Here we explicitly show the leading contribution to the soft part \hat{S}_N which is of order $Q^3=M^2$, as would be expected from Weinberg's power counting. The ellipsis represents higher-order terms. For illustrative purposes, it is useful to sum up the series of soft contributions. This can be carried out by noting that in the present case, after our exchange of the integration and summation, an ℓ^2 in the numerator of any integrand can be replaced with m^2 in dimensional regularization. Then the exact soft part of the one-loop self-energy diagram is

$$\hat{S}_N(k) = \frac{3g_A^2}{4f^2} i^{4-d} \int \frac{d^d \ell}{(2\pi)^d} \frac{(2k - \ell + m) \gamma (\ell + M) m^2}{(\ell^2 - m^2 + i)(2k^2 - \ell^2 + 2k^2 M^2 + m^2 + i)} : \quad (32)$$

Introducing

$$\Delta = \frac{1}{2} \frac{1}{k^2 - M^2 - m^2} ; \quad (33)$$

which is of order Q , the integral of Eq. (32) in the case $|j| < m$ can be written

$$\begin{aligned} \hat{S}_N(k) = & \frac{3g_A^2}{2(4-f)^2} \frac{m^2}{k^2} (\ell + M) - \frac{k^2 - M^2}{k^2} \Delta \frac{1}{2} \frac{q}{m^2} \frac{1}{\ell^2} \cos^{-1} \frac{m}{m} \\ & \frac{3g_A^2}{8(4-f)^2} \frac{k^2 - M^2}{k^2} (m^2 - 2\ell^2) \Delta + \frac{2! m^2}{k^2} (\ell + M) - 32^{-2} L + \ln \frac{m^2}{2} ; \end{aligned} \quad (34)$$

where

$$L = \frac{1}{32\pi^2} \frac{2}{d-4} + \frac{1}{2} \ln 4 ; \quad (35)$$

with Euler's constant $\gamma = 0.577$.

In the modified minimal subtraction (\overline{MS}) renormalization scheme, we obtain the renormalized soft part \hat{S}_N by including counterterm contributions (CTCs) to remove the term proportional to L in Eq. (34). We can further ensure that the pole of the nucleon propagator is at the physical mass with unit residue by additional on-shell mass and wavefunction counterterm subtractions as detailed in Eq. (70) below. These CTCs can clearly be expanded in an infinite power series in $(k^2 - M^2)/M^2$. Thus, the divergences appear to all orders in the Q^2/M^2 expansion. The divergences can be removed by introducing counterterms of the form $\frac{1}{M^{n-1}} \overline{N}(i\partial - M)^N$ with n an integer. However, we note that we may use the nucleon equation of motion [20,25,26] to eliminate the above counterterms in favor of interaction terms involving multiple pions and nucleons.

We may obtain the leading order Q^2/M^2 contribution to Eq. (34) by approximating $\sqrt{k^2 - M^2} = (2M)^{1/2}$ and setting $\frac{p}{k^2} \rightarrow \frac{p}{M^2}$ in the denominators. It is not possible to expand this leading-order expression further since the square root and inverse cosine functions in the equation involve $\sqrt{m^2}$ and m which are of the same order. Thus, we cannot absorb this soft part into the parameters of the lagrangian. This result is consistent with the expectation that the parameters should contain only high-energy contributions.

The hard part of the self energy can also be evaluated directly. We find

$$\begin{aligned} (i\hat{S})_N(k) &= \frac{3g_A^2}{4f^2} i^{4-d} \int \frac{d^d v}{(2\pi)^d} \frac{(\not{v} - \not{k})(\not{v} - \not{M})(\not{v} - \not{k})}{(v^2 - M^2 + i)(2k - v)^2 (k^2 - M^2 + m^2 + i)} \\ &= \frac{3g_A^2}{4(4-f)^2} M^2 \not{M} + \frac{k^2 + M^2}{2k^2} \not{k} \left[32\pi^2 L + \ln \frac{M^2}{2} \right] \\ &\quad + \frac{3g_A^2}{4(4-f)^2} \frac{p}{k^2} \not{k} \left[\frac{k^2 - M^2}{k^2} \right] \not{k} \frac{m^2}{k^2} (\not{k} + \not{M}) \\ &\quad \left[32\pi^2 L + \ln \frac{M^2}{2} \right] + \sum_{j=1}^{\infty} \frac{2}{21} \frac{1}{1} \frac{(\not{k}^2 - m^2)^j}{(\not{k}^2 - m^2)^j} : \end{aligned} \quad (36)$$

Notice that the integral in the first equation of (36) is dominated by poles at momenta of $O(M)$. The final result can indeed be expanded in powers of $(k^2 - M^2)/M^2$ and thereby

removed by CTCs. If this were not done the power counting would be spoilt since the first term of the result is of $O(M)$ and the second is of $O(Q^2=M^2)$, which can be contrasted with $O(Q^3=M^2)$ for the soft part.

While our procedure is plausible, a general proof would require consideration of diagrams of arbitrary complexity. Here we restrict ourselves to one-loop order for which it is easy to see that our procedure gives the same result as HBChPT. Indeed, the expansion of the baryon propagator in Eq. (30) generates the same effects as integrating out the heavy components of the baryon fields in HBChPT. For our example of the nucleon self-energy we can make the connection with HBChPT by introducing in Eq. (31) the four velocity v such that $k = Mv + q$ with $v \cdot v = 1$. Projecting onto the light components by inserting the projection operators $\frac{1}{2}(1 + \not{v}) = \frac{1}{2}(1 + \not{v})^2$ fore and aft, and noting that

$$\frac{1}{2}(1 + \not{v}) \not{S} \frac{1}{2}(1 + \not{v}) = 2 \not{v} \frac{1}{2}(1 + \not{v}) ; \quad (37)$$

where $S = \frac{1}{2}i \not{S} \not{v}$, we find

$$\frac{1}{2}(1 + \not{v}) \hat{S} \not{N}(k) \frac{1}{2}(1 + \not{v}) = \frac{1}{2}(1 + \not{v}) \frac{3g_A^2}{f^2} i \not{S} \frac{d^d v}{(2\pi)^d} \frac{(\not{v} \not{S})}{v^2} \frac{1}{m^2 + i0} \frac{1}{v \cdot q - v^2 + i0} ; \quad (38)$$

This is a well-known expression which follows directly from the Feynman rules of HBChPT [13,16]. Our expression for the soft part, Eq. (34), when projected onto the light components yields in leading order (or equivalently in the infinite nucleon mass limit) the result of Bernard et al. [13,31] obtained in HBChPT.

Mojzis [16] has recently calculated diagrams for N scattering using HBChPT with just pions and nucleons up to one-loop Q^3 order. The results of our calculation, given in the Appendix, agree with his (modulo differences in the parameterization of U and the treatment of finite terms arising from the product of a $(d-4)$ factor with the $1=(d-4)$ pole, see below). For simplicity our examples have involved the nucleon propagator, but we emphasise that the delta propagator appearing in loop diagrams (denoted by an open box in Figs. 9 and 10

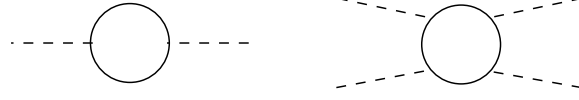


FIG. 2. Sample diagrams with baryon loops not directly connected to external baryon lines.

below) is treated in exactly the same way. This is necessary to preserve the power counting and it gives results which agree with the HBChPT approach of Hemmert et al. [32].

B. Fermion Loops and Power Counting

Fermion loops were not discussed in the preceding section. We notice that there are no fermion loops in HBChPT after integrating out the heavy field components. Here we show that fermion loops have vanishing soft parts in our approach so that they can be ignored. First consider fermion loops that are not directly connected to external fermion lines, such as those in Fig. 2. We will work with nucleons for simplicity, although similar arguments can be given for π 's. If we generalize our previous rules by taking the loop momentum to be of $O(Q)$, we can expand the propagators in the form

$$G(p) = \frac{1}{M^2} \not{p} + M \left(1 + \frac{p^2}{M^2} + \dots \right) : \quad (39)$$

In dimensional regularization $\int^R d^d p = 0$ so the soft part vanishes. Alternatively, a direct calculation of the loop integrals with the standard Feynman rules can be used to show that the contributions of the diagrams can be expanded in a power series in terms of small pion momenta (a $Q \ll M$ expansion) and can thus be absorbed in the lagrangian. In other words there is no soft part.

Next we discuss fermion loops generated from four (or more) fermion vertices, such as those in Fig. 3. These can be considered to arise from Fig. 4 by shrinking the heavy boson lines to points. Since the momentum transfers through the boson lines must be small if it is feasible to integrate out the heavy bosons, the arguments given in connection with Fig. 2

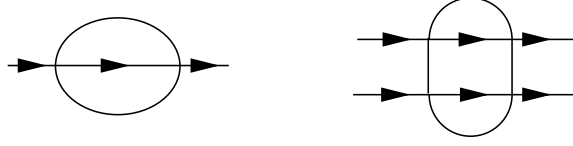


FIG . 3. Sample diagrams with baryon loops involving four baryon vertices.

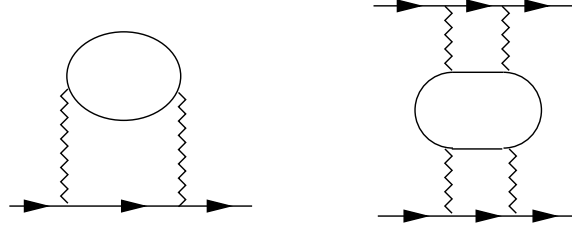


FIG . 4. Diagrams which yield Fig. 3 when the heavy boson propagators, represented by wiggly lines, are shrunk to a point.

can also be applied here. Therefore the soft parts vanish. Alternatively, this may be shown directly by taking the loop momenta to be of $O(Q)$, using Eqs. (30) and (39), together with the relation

$$\int^Z d^d \lambda \frac{(\lambda^2)^m}{(2k - \lambda + i^n)} = 0 ; \quad (40)$$

where λ is independent of λ . Equation (40) is valid in dimensional regularization for any integers m and n (see Ref. [30] for example).

Finally, we need to consider the special case where an N -baryon scattering process contains an N -baryon intermediate state. A simple example is given in Fig. 5. We note that if we consider the four-fermion interaction in terms of the exchange of a heavy boson, as before, this diagram will not contain a baryon loop. As Weinberg noticed [20], there is an infrared divergence in Fig. 5 for on-shell nucleons at zero kinetic energy. Indeed, the amplitude is proportional to

$$\int^Z d^4 \lambda P_1(\lambda) G(p_1 + \lambda) G(p_2 - \lambda) = \int^Z d^4 \lambda \frac{P_2(\lambda)}{2p_1 \cdot \lambda + \frac{1}{2}p^2 - M^2 + i}$$

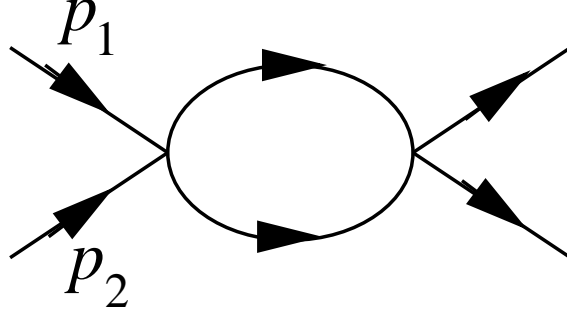


FIG. 5. A two-baryon reducible diagram that needs special treatment.

$$\frac{1}{2p_2 \sqrt{p^2 + \frac{M^2}{2}} + i} + \dots; \quad (41)$$

where $P_1(\sqrt{s})$ and $P_2(\sqrt{s})$ are polynomials in the loop momentum \sqrt{s} . We have taken \sqrt{s} to be of order Q and expanded the integrand in the manner of Eq. (30). The contour of integration is pinched between the two poles at $\sqrt{s} = \pm i$ for $p = p_2 = (M; 0)$, and so cannot be distorted to avoid these singularities. Of course, this just signals that our expansion fails. The way out of this difficulty has also been given by Weinberg: we should consider only N -baryon irreducible diagrams for N -baryon scattering processes. The reducible diagrams are summed up with the N -body Bethe-Salpeter equation, the kernel of which is obtained from the irreducible diagrams.

Even in one-baryon processes, such as N scattering, singular behavior can arise when an intermediate π goes on shell. A similar remedy is followed: first calculate the irreducible self-energy diagrams to a certain order, then sum up the string of reducible diagrams containing arbitrary numbers of self-energy insertions (see Sec. IV).

We can now discuss the power counting for irreducible diagrams that do not contain fermion loops. According to Eq. (30) the leading order of a baryon propagator is Q^{-1} and according to Rule 1 the loop momentum is of order Q . Thus all the power-counting arguments of Weinberg [20] carry over. It follows that the leading order of a Feynman diagram with L loops, E_N external baryon lines is Q^{-L} with

$$= 2 + 2L - \frac{1}{2}E_N + \sum_i^X V_i d_i + \frac{1}{2}n_i - 2 ; \quad (42)$$

where V_i is the number of vertices of type i characterized by n_i baryon fields and d_i pion derivatives or meson factors. (We used the quantity $d_i + \frac{1}{2}n_i$ to characterize terms in the lagrangian in Sec. II.) In general each diagram may contribute at orders beyond the leading Q order.

IV. PION-NUCLEON SCATTERING

We apply our formalism to πN scattering and calculate the T matrix to $O(Q^3)$. The Q^3 amplitude is obtained from tree diagrams constructed from our lagrangian $L_2 + L_3 + L_4$ and one-loop diagrams constructed from L_2 . Following the standard notation of Hohler [33] and Ericson and Weise [34] we write the T matrix as

$$T_{ba} = h_b T_j j_a i = T^+_{ab} + \frac{1}{2} [b; a] T^- ; \quad (43)$$

where the isospin symmetric and antisymmetric amplitudes are

$$T = A + \frac{1}{2} (q + q^0) B ; \quad (44)$$

Here, as shown in Fig. 6(a), q and q^0 are the c.m. momenta of the incoming and outgoing pions with isospin labels a and b respectively. The c.m. momenta of the incoming and outgoing nucleons are labelled p and p^0 respectively. The amplitudes A and B are functions of the Mandelstam invariants $s = (p + q)^2$, $t = (q - q^0)^2$, and $u = (p - q^0)^2$.

A. Tree-level Contact Terms & Nucleon Exchange

In Fig. 6 we show the tree level Feynman diagrams arising from the contact terms and from one nucleon exchange, with the crossed diagram for the latter suppressed. The vertex in Fig. 6(a) arises from any of the interactions in L_3 and L_4 (except for the π_1 and π_6 terms), as well as the Weinberg term $\bar{N} \gamma_5 N$. It is straightforward to obtain the amplitudes arising from the contact terms. The results are

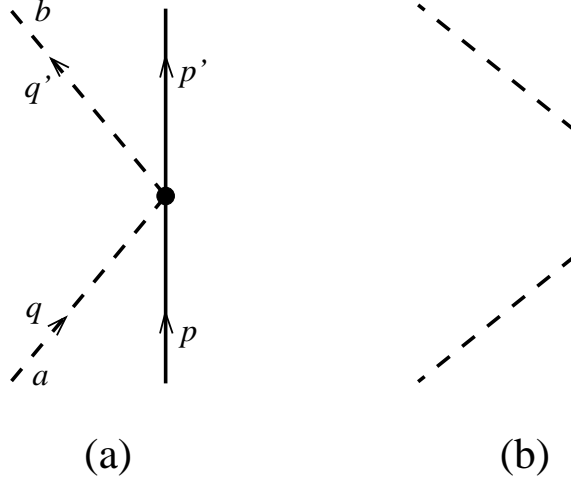


FIG. 6. Tree-level diagrams for NN scattering. (a) contact interactions; (b) nucleon exchange with the cross diagram suppressed.

$$A_C^+ = \frac{1}{M f^2} \left(2m^2 t + 4m^2 + \frac{4}{8M^2} (s - u)^2 \right); \quad (45)$$

$$B_C^+ = \frac{1}{4M^2 f^2} (1 - 2t) (s - u); \quad (46)$$

$$A_C = \frac{1}{2M f^2} (s - u); \quad (47)$$

$$B_C = \frac{1}{2f^2} (1 + 4t) - \frac{1}{M^2 f^2} \left(\frac{1}{2} t + 4m^2 \right) - \frac{5}{16M^2} (s - u)^2; \quad (48)$$

The parameters here will absorb the divergences arising from the one-loop diagrams. They depend on the scale of dimensional regularization, μ , in such a way that the complete T-matrix is μ -independent. The contributions from nucleon exchange shown in Fig. 6(b) are well-known, see for example Ref. [33]. Including the crossed diagrams, we have

$$A_N^+ = \frac{g_A^2}{f^2} M; \quad (49)$$

$$B_N^+ = \frac{g_A^2}{f^2} M^2 \left(\frac{1}{u} - \frac{1}{M^2} \right) - \frac{1}{s - M^2}; \quad (50)$$

$$A_N = 0; \quad (51)$$

$$B_N = \frac{g_A^2}{2f^2} - \frac{g_A^2}{f^2} M^2 \left(\frac{1}{s - M^2} + \frac{1}{u - M^2} \right); \quad (52)$$



FIG. 7. One-loop self-energy diagrams. The open box represents the free propagator.

Here we have used the exact nucleon propagator, although it could be expanded in chiral orders as in Ref. [16]. The difference would appear beyond $O(Q^3)$ which is the level of precision of the present calculation. Note that identification of what is to be included to $O(Q^3)$ is model dependent since the hard momentum scale could be M_π , M_ρ , the average mass M , or $4\pi f$. Results obtained with different choices will differ at $O(Q^4)$ and beyond, but this should not affect the quality of the fit to the data so that we shall simply write our expressions in convenient form.

B. Exchange

When the π appears as an intermediate state for NN scattering, the tree-level T -matrix diverges at $s = M_\pi^2$ so the power counting fails. As argued earlier, we expect the power counting to work only for irreducible diagrams. Thus we evaluate the one-particle irreducible self-energy diagrams which, to one-loop order, are those of Fig. 7. Diagrams containing one or more self-energy insertions are then summed to replace the free propagator by the dressed propagator which is finite.

We start by writing down the free propagator

$$G^0(k) = \frac{1}{\not{k} - M + i} = g + \frac{1}{3} + \frac{1}{3M} (\not{k} - k) + \frac{2k \cdot k}{3M^2} : \quad (53)$$

This may be recast in terms of the spin projection operators [35,36] as

$$G^0(k) = \frac{1}{\not{k} - M + i} (P^{3=2}) - \frac{1}{3M} (P_{12}^{1=2} + P_{21}^{1=2}) + \frac{2}{3M^2} (\not{k} + M) (P_{22}^{1=2}) ; \quad (54)$$

where

$$\begin{aligned}
(P^{3=2}) &= g \left(\frac{1}{3} + \frac{1}{3k^2} (k \cdot k) \right) \not{k} - \frac{2}{3k^2} k \cdot k ; \\
(P_{11}^{1=2}) &= \frac{1}{3} - \frac{1}{3k^2} (k \cdot k) \not{k} - \frac{1}{3k^2} k \cdot k ; \\
(P_{12}^{1=2}) &= \frac{1}{3k^2} (k \cdot k + k \cdot k) ; \\
(P_{21}^{1=2}) &= \frac{1}{3k^2} (k \cdot k - k \cdot k) ; \\
(P_{22}^{1=2}) &= \frac{1}{k^2} k \cdot k ;
\end{aligned} \tag{55}$$

The spin projection operators obey the orthogonality relations

$$P_{ij}^I P_{kl}^J = \delta_{IJ} \delta_{jk} P_{il}^I ; \tag{56}$$

The dressed propagator contains any number of irreducible self-energy insertions:

$$G = G^0 + G^0 \Sigma G^0 + G^0 \Sigma G^0 \Sigma G^0 + \dots ; \tag{57}$$

where $\Sigma(k)$ is the self-energy. Since $G^0(k)$ and $k \cdot G^0(k)$ do not contain a pole at $k^2 = M^2$, we conclude from Eq. (57) that the tensor terms in $\Sigma(k)$ constructed from \not{k} and $k \cdot k$ generate non-pole terms in the dressed propagator G . It is not hard to see that these terms start to contribute to the T-matrix at order Q^5 . We can thus greatly simplify our calculations by noting that in the self-energy tensor

$$\Sigma(k) = \Sigma(k)g + \dots ; \tag{58}$$

the aforementioned tensor terms, represented by the ellipsis, can be neglected. Renormalizing in the \overline{MS} scheme we obtain $\overline{\Sigma}^{MS}$. We make additional on-shell mass and wavefunction counterterm subtractions such that, when the imaginary part of the self-energy is neglected, the pole of the propagator lies at the physical mass with unit residue. Thus, the renormalized self-energy is

$$\Sigma^{ren}(k) = \overline{\Sigma}^{MS}(k) - \frac{\partial}{\partial \not{k}} \overline{\Sigma}^{MS}(k) \Big|_{\not{k}=M} \not{k} - M ; \tag{59}$$

where $<$ refers to the real part. Breaking the self-energy into real and imaginary parts we obtain the dressed propagator

$$G(k) = \frac{k^2 + M^2}{k^2 - M^2} \frac{1}{(k^2 + iM)} (P^{3=2}) - \frac{1}{3M} (P_{12}^{1=2} + P_{21}^{1=2}) + \frac{2}{3M^2} (k^2 + M^2) (P_{22}^{1=2}) ; \quad (60)$$

We have ignored $O(Q^3)$ contributions to the non-pole terms which involve $P^{1=2}$ since, as we have remarked, they do not contribute to the N T-matrix until $O(Q^5)$. Also in the numerator of the pole term in Eq. (60) we have neglected terms of $O(Q^3)$, which contribute to the N T-matrix at $O(Q^4)$. It is convenient to write the real part of the "polarization" as a function of $k^2 = \frac{1}{2}(k^2 - M^2) = M^2$, with the mean baryon mass $M = \frac{1}{2}(M_1 + M_2)$. To $O(Q^3)$ the two diagrams of Fig. 7 yield

$$\begin{aligned} (k^2) = & \frac{4 h_A^2 M}{3 (4 - f)^2} \left[\frac{2}{k^2} m^2 J(k^2) - \frac{2}{k^2} m^2 J(0) \right. \\ & \left. - 3 J(0) - k^2 + m^2 + m^2 \ln \frac{m^2}{2} \left(\frac{1}{k^2} - \frac{1}{m^2} \right) \right] \\ & - \frac{25 h_A^2 M}{27 (4 - f)^2} \left[\frac{h}{k^2} \left(\frac{1}{k^2} - \frac{1}{m^2} \right) - m^2 J(k^2) \right] \\ & - m^3 - m^2 \left[1 + \ln \frac{m^2}{2} \left(\frac{1}{k^2} - \frac{1}{m^2} \right) \right] ; \quad (61) \end{aligned}$$

where the function J is defined in the Appendix. For the energies considered here the imaginary part arises from the first diagram of Fig. 7 which gives

$$(k^2) = \frac{h_A^2}{12M} \frac{k^2}{k^4 (4 - f)^2} \frac{h}{k^2 + M^2 + 2M} \frac{h}{(k^2 - M^2)^2} - \frac{h}{(k^2 + 3M^2)m^2} \frac{1}{(k^2 - M^2)^2 - 4k^2 m^2} ; \quad (62)$$

We have evaluated Γ up to $O(Q^4)$ because this significantly improves the accuracy of the decay width, $\Gamma(k^2 = M^2)$. In fact the error is negligible when compared with an exact evaluation using tree-level coupling, $g_N = h_A M = f$ (for the coupling to $O(Q^2)$ see Eq. (83) below). Specially this is [33]

$$\Gamma_{\text{exact}} = \frac{g_N^2}{12} \frac{h_A^3}{M^2 M} M + \frac{h_A^3}{h_A^2 + M^2} ; \quad (63)$$

where $h_A^2 = (4M^2 - m^2)(k^2 - m^2) = (4M^2)$.

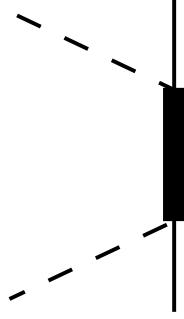


FIG. 8. The exchange diagram with the dressed propagator represented by a solid box.

Using the dressed propagator of Eq. (60), the exchange contribution to the real part of the T-matrix, pictured in Fig. 8, is

$$T^{ba} = (ab - \frac{1}{4} [b; a]) \frac{h_A^2}{9M^2 f^2 S} 6M^2 R(s) s [\frac{1}{2} (s; t) + \frac{1}{2} (s; t) q] \\ (s - M^2 + m^2)^h M (s - M^2) + (M + 2M) m^2 + (s - M^2 + 2M M + m^2) q^i ; \quad (64)$$

where we define $\frac{1}{2} (s - M^2) = M$ and the real part of the propagator is

$$R(s) = \frac{s - M^2}{[s - M^2 - ()^2 + M^2 - 2(s)]} ; \quad (65)$$

We do not expand the propagator for the reason given at the end of Subsec. A. The definitions of the functions $\frac{1}{2}$ and $\frac{1}{2}$ are

$$\frac{1}{2}(s; t) = 2M^h m^2 - \frac{1}{2} t - \frac{1}{3} (s - M^2)^i - \frac{(s - M^2 + m^2)^h}{6s} M (s - M^2) + m^2 (M + 2M)^i ; \\ \frac{1}{2}(s; t) = \frac{2}{3} m^2 - \frac{1}{2} t + \frac{4}{3} M M - \frac{(s - M^2 + m^2)}{6s} s - M^2 + 2M M + m^2 ; \quad (66)$$

To this should be added the result for the cross diagram which is obtained from the above by the replacement $s \rightarrow u$ and the interchanges $a \leftrightarrow b$ and $q \leftrightarrow q$.

C. One-Loop Diagrams

A set of one-loop diagrams that contribute to the N T-matrix at $O(Q^3)$ is shown in Fig. 9. Here we can use the free propagator since no singularities are generated in the

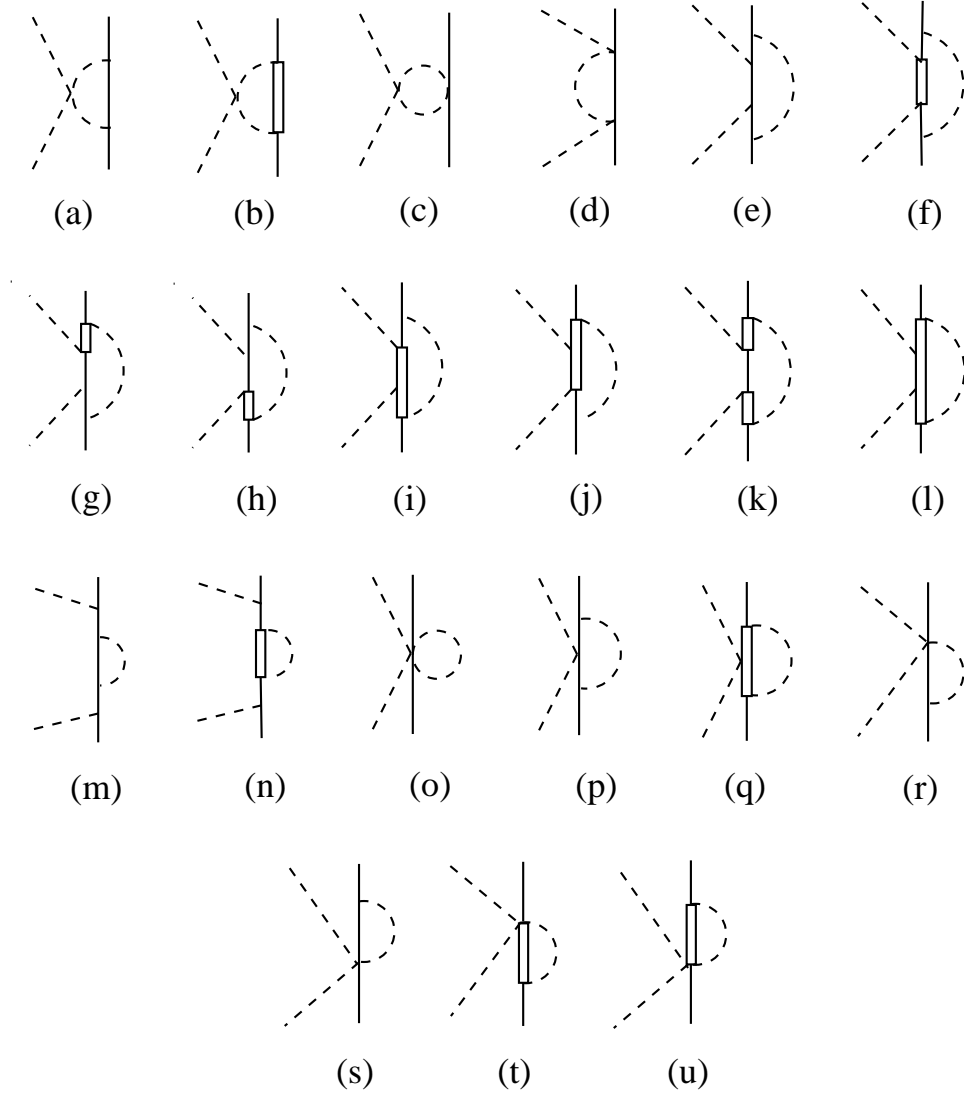


FIG. 9. A set of one-loop diagrams which contribute at $O(Q^3)$. Crossed diagrams for (d) to (n) are not shown.

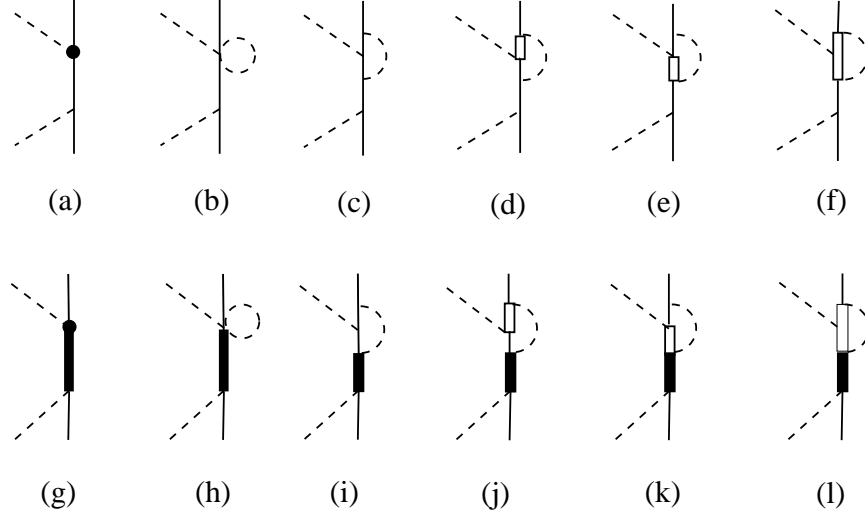


FIG. 10. Diagrams with one-loop vertices which contribute at $O(Q^3)$. Crossed diagrams are not shown. The solid circle in (a) and (g) refers to γ_1 and γ_6 vertices, respectively. Each diagram implicitly includes its counterpart where the lower vertex is dressed.

Matrix. A covariant expansion of the propagators, as well as the nucleon propagators, is made in the manner discussed in Sec. IIIA so that the denominators are of order Q . These propagators are denoted by open boxes in Fig. 9.

As an illustration, we calculate the matrix for Fig. 9(e). Using the standard Feynman rules, we find

$$\bar{u}(p^0) T_{9e}^{ba} u(p) = \frac{g_A^4}{16f^4} i \epsilon^{\mu\nu\alpha\beta} \frac{d^\mu \gamma^\nu}{(2\pi)^d} \frac{1}{\omega^2} \frac{1}{m^2 + i} \bar{u}(p^0) \gamma_5 \epsilon^{\mu\nu\alpha\beta} (p^0 + \gamma) \not{q} \gamma_5 \epsilon^{\mu\nu\alpha\beta} (p + q + \gamma) \not{q} \gamma_5 \epsilon^{\mu\nu\alpha\beta} (p + \gamma) \gamma_5 u(p) : \quad (67)$$

Noting that $p^0 = p + q - \not{q}$, and that q , q^0 , and γ are of order Q , we can expand the nucleon propagators as in Eq. (30) and select the leading terms. Then the contribution to $O(Q^3)$ is

$$\bar{u}(p^0) T_{9e}^{ba} u(p) = \frac{3g_A^4}{16f^4} i \epsilon^{\mu\nu\alpha\beta} \frac{d^\mu \gamma^\nu}{(2\pi)^d} \frac{\bar{u}(p^0) \gamma_5 \not{p}^0 \not{M} \not{q} \not{p} + M \not{q} \not{p} \not{M} \gamma_5 \epsilon^{\mu\nu\alpha\beta} \frac{1}{6} [\gamma^b; \gamma^a] u(p)}{(\omega^2 - m^2 + i)(2p \cdot \gamma + i)(2p \cdot \gamma + 2p \cdot q + i)} \quad (68)$$

As in Sec. III, we can cast this in HBChPT form. Setting $p = Mv$ for the incoming nucleon, we easily obtain

$$\bar{u}(p^0) T_{9e}^{ba} u(p) = \frac{3g_A^4}{f^4} i^{4-d} \frac{d^d v}{(2)^d} \frac{\bar{u}(p^0) (\not{v} - \not{S})(q^0 - S)(q - S)^b \frac{1}{6} [\not{v}; \not{a}] u(p)}{(\not{v}^2 - m^2 + i)(\not{v} - \not{v} + i)(\not{v} - \not{v} + \not{v} - q + i)} \quad (69)$$

It is tedious, but straightforward to evaluate the numerators of Eqs. (68) or (69) and carry out the integration using the results in the Appendix. We use the modified minimal subtraction scheme (\overline{MS}) to remove the singularities and the resulting real part of the T-matrix is listed in Eq. (A20). Note that divergent terms proportional to $1/(d-4)$ involves polynomials in the variables and so they can be absorbed into the contact-term contributions. For the same reason, we can absorb finite polynomial terms obtained from the product of a $1/(d-4)$ singularity and $(d-4)$ factors. The latter may be generated from d-dimensional matrix algebra or from integration of tensor factors such as $v^\mu v^\nu$ in the numerator of the integrand. The above simplification has been exercised for the results listed in the Appendix.

The real parts of the T-matrix for the remaining diagrams of Fig. 9 are evaluated in like fashion to $O(Q^3)$ and listed in the Appendix. Note that the diagrams in Fig. 9 (m) and (n) involve the nucleon one-loop self-energy which is real for the energies of interest here. As with the Σ , we renormalize in the \overline{MS} scheme to obtain $\overline{M_N^S}$ and make additional on-shell mass and wavefunction counterterm subtractions. Thus, the renormalized self-energy is

$$\Sigma_N^{\text{ren}}(k) = \overline{M_N^S}(k) - \overline{M_N^S}(k) \Big|_{\not{k}=M} - \frac{\partial}{\partial \not{k}} \overline{M_N^S}(k) \Big|_{\not{k}=M} \not{k} \quad (70)$$

Since these diagrams do not give singular contributions to the T-matrix we do not sum the self-energy insertions.

We also need to evaluate the vertex modification diagrams shown in Fig. 10. The propagators denoted by open boxes have the same meaning as for Fig. 9. However there are now cases where the Σ can go on shell for which we use the dressed propagator of Eq. (60), as indicated by the solid box. For the diagrams in Fig. 10 (i) and (j) the contributions

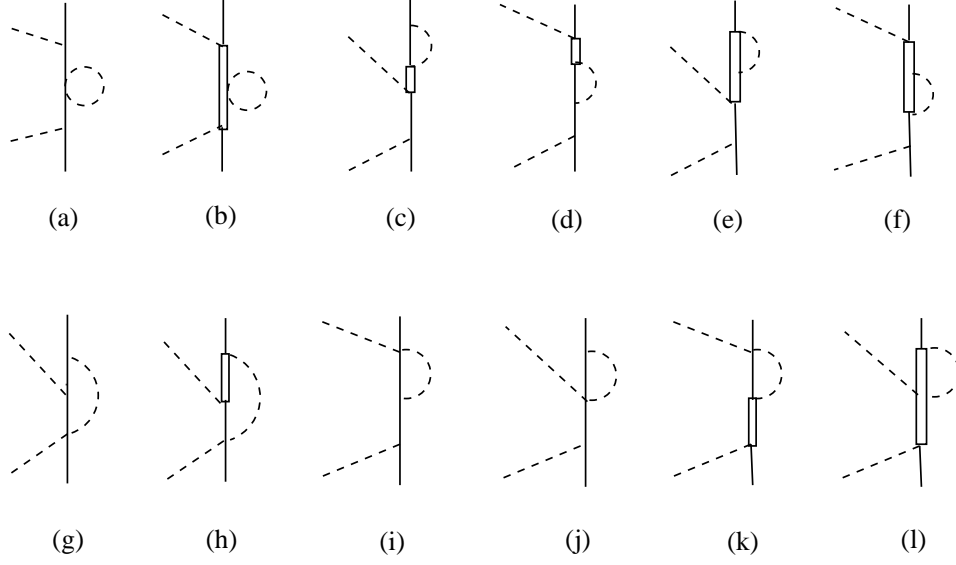


FIG. 11. One-loop diagrams which either vanish, (a) to (f), or do not contribute at $O(Q^3)$, (g) to (l). Crossed diagrams and diagrams with the time ordering reversed are not explicitly shown.

proportional to $\Gamma_R(s)$ vanish at the pole where $s = M^2$ (and so $\Gamma_R = 0$). As a result, at the pole there are important contributions to the T-matrix coming from the imaginary part of the N vertex. These contributions actually are of $O(Q^1)$ for energies very close to the resonance ($j = j_{\text{res}}$). Thus, we keep the leading-order pole corrections in Eqs. (A41) and (A42). We have also considered the next-to-leading order ($O(Q^2)$) pole corrections for Fig. 10 (i) and (j), as well as the leading $O(Q^3)$ pole correction to the exchange diagram of Fig. 8. These gave a very small effect and were not included in the final result. The expressions for the vertex modification contributions to the T-matrix are also listed in the Appendix. We reiterate that our expressions for diagrams that do not involve the ρ propagator agree with those recently given by Mojzis [16]. Finally we show in Fig. 11 a set of one-loop diagrams which do not need to be considered. The top row, 11 (a) { (f), is identically zero due to the vertex structure or to violation of isospin conservation. The lower row, 11 (g) { (l), does not contribute to $O(Q^3)$. This is a welcome simplification.

From the real part of the T-matrix the real part of the elastic scattering amplitude, f , is obtained by the standard partial wave expansion [37]. Here the isospin-spin partial wave

channels are labelled by $(l; 2I; 2J)$ with l the orbital angular momentum, I the total isospin, and $J = l \pm \frac{1}{2}$ the total angular momentum. The phase shifts are then given by

$$\delta_{lIJ} = \frac{1}{2} \sin^{-1} \left(\frac{f_{lIJ}}{k} \right) \quad (71)$$

D. Pion {Nucleon} Term

We may obtain the nucleon term from the Feynman-Hellman theorem,

$$\frac{\partial M}{\partial m^2} = - \frac{1}{2} \frac{\partial}{\partial m^2} \left(\frac{M}{m^2} \right) \quad (72)$$

Working out the nucleon self-energy up to one-loop Q^3 order, we find

$$M = M_0 + \frac{4}{3} \frac{g_A^2}{M} m^2 + \frac{3}{2} \frac{g_A^2}{(4f)^2} m^3 + \frac{8}{3} \frac{h_A^2}{(4f)^2} (m^2 - m^2) J\left(\frac{m^2}{\Lambda^2}\right) + \frac{1}{2} m^2 \ln \frac{m^2}{\Lambda^2} \quad (73)$$

where the function J is defined in the Appendix and M_0 is the "bare" nucleon mass defined to be independent of the pion mass. Note that, as in HB χ PT, contact terms proportional to Q^3 are needed to absorb the divergences and m dependence associated with the degrees of freedom. We have not specified these explicitly, hence our M_0 depends on Λ and m . The term up to $O(Q^3)$ is then

$$(0) = \frac{4}{3} \frac{g_A^2}{M} m^2 + \frac{9}{4} \frac{g_A^2}{(4f)^2} m^3 + \frac{8}{3} \frac{h_A^2 m^2}{(4f)^2} \ln \frac{m^2}{\Lambda^2} + \frac{3}{2} J\left(\frac{m^2}{\Lambda^2}\right) \quad (74)$$

Note that the m dependence in $J\left(\frac{m^2}{\Lambda^2}\right)$ may be absorbed in Λ^2 so that Λ is independent of m .

The isospin even on-shell amplitude $\overline{D}^+(\pi; t)$ at the Cheng-Dashen point can be related to the N term, $(2m^2)$, as follows [38]:

$$f^2 \overline{D}^+(\pi; t=2m^2) = (2m^2) + O(m^4) \quad (75)$$

where $\pi = (s-u)/(4M)$ and \overline{D}^+ is obtained from

$$D^+(\pi; t) = A^+(\pi; t) + B^+(\pi; t) \quad (76)$$

by the subtraction of the nucleon pole term which comes from the tree diagram in Fig. 6 (b) and the one-loop diagrams in Figs. 10 (a) to 10 (f). At the Cheng-Dashen point only Figs. 8, 9 (a), 9 (b) and Figs. 9 (r) to 9 (u) contribute to the term. Using the results for the T-matrix as given in the Appendix, we find

$$\begin{aligned}
(2m^2) \quad (0) = & \frac{3}{4} \frac{q_A^2}{(4-f)^2} m^3 + \frac{h_A^2 m^4}{3M^2} \\
& + \frac{2}{3} \frac{h_A^2 m^2}{(4-f)^2} \left(\frac{q}{4} \frac{1}{m^2} \ln^0 \frac{0}{m} + \frac{v}{m^2} \frac{1}{m^2} \right) \\
& + \int_0^1 dx \frac{2}{m^2 (1-2x+2x^2)} \ln \frac{q}{m^2 (1-2x+2x^2)} : \quad (77)
\end{aligned}$$

Note that since we count Γ to be of order Q the second term on the right is of the same Q^3 order as the other terms. Equation (77) agrees with the result of Bernard et al. [13,39] who obtain this expression from HBChPT and dispersion relations. (Their integral is in a form which is slightly different from ours, but both integrals give the same numerical result.)

E. NN and N Couplings

The NN vertex up to one-loop order consists of the tree vertex generated from the axial a term in the lagrangian and the one-loop diagrams shown in the upper part of Figs. 10 (a) to (f). Following our procedure, we can straightforwardly calculate the one-loop vertex function $\Gamma^a(k; k^0; q)$, where k (k^0) is the incoming (outgoing) momentum of the nucleon and $q = k^0 - k$ is the momentum transfer. The NN coupling for on-shell nucleons is obtained by sandwiching this vertex function between nucleon spinors:

$$\bar{u}(k^0) \stackrel{a}{\sim} (k; k^0; q) u(k) = g_{NN}(q^2) \bar{u}(k^0) \stackrel{5}{\sim} u(k) : \quad (78)$$

W e nd

$$g_{NN}(q^2) = g_{NN}(0) + O(q^2 Q^2); \quad (79)$$

which implies that the difference between the on-shell pion coupling $g_{NN}(\mathbf{m}^2)$ and $g_{NN}(0)$ is of $\mathcal{O}(Q^4)$. This justifies the usual assumption of a small variation in $g_{NN}(q^2)$ between

$q^2 = 0$ and $q^2 = m^2$ when the Goldberger-Treiman relation is derived [40]. To $O(Q^2)$ we obtain

$$\begin{aligned} g_{NN}(0) = & \frac{M g_A}{f} \left[1 - \frac{2}{3} \frac{m^2}{(4f)^2} \ln \frac{m^2}{2} + \frac{g_A^2}{6} \frac{m^2}{(4f)^2} \left(1 + \frac{3}{2} \ln \frac{m^2}{2} \right) \right. \\ & + \frac{64}{27} \frac{h_A^2}{(4f)^2} m^3 + \frac{m^2}{2} J\left(\frac{m^2}{2}\right) + \frac{1}{2} m^2 \ln \frac{m^2}{2} \\ & \left. + \frac{200}{243 g_A} \frac{h_A^2 \tilde{h}_A}{(4f)^2} m^2 - \frac{m^2}{3} J\left(\frac{m^2}{2}\right) - \frac{3}{2} m^2 \ln \frac{m^2}{2} + O(Q^3) \right] : \quad (80) \end{aligned}$$

Notice that γ_1 absorbs the divergences and q -dependence arising from the one-loop vertices. With the parameters obtained from fits to the NN phase shifts Eq. (80) allows a test of the Goldberger-Treiman relation.

Similarly, we can calculate the NN vertex from the tree-level h_A term and the one-loop diagrams shown in the upper part of Figs. 10 (g) to (l). Here, in the vertex function $\Gamma^a(k; k^0; q)$ the label k now refers to the incoming momentum. The NN coupling is obtained by sandwiching this vertex function between the nucleon spinor and the spinor, $u(k)$:

$$\bar{u}(k^0) \Gamma^a(k; k^0; q) u(k) = g_{NN}(q^2) \bar{u}(k^0) q \cdot T^a u(k) : \quad (81)$$

We find

$$g_{NN}(q^2) = g_{NN}(0) + O(q^2 Q^2) ; \quad (82)$$

where

$$\begin{aligned} g_{NN}(0) = & \frac{M h_A}{f} \left[1 - \frac{2}{3} \frac{m^2}{(4f)^2} \ln \frac{m^2}{2} \right. \\ & + \frac{2}{3} \frac{1}{(4f)^2} g_A^2 + \frac{1}{9} h_A^2 + \frac{25}{81} \tilde{h}_A^2 m^2 J\left(\frac{m^2}{2}\right) + \frac{1}{2} m^2 \ln \frac{m^2}{2} \\ & + \frac{2}{3} \frac{1}{(4f)^2} g_A^2 + \frac{25}{81} \tilde{h}_A^2 m^3 - \frac{25 g_A \tilde{h}_A m^2}{54 (4f)^2} \left(1 + \frac{3}{2} \ln \frac{m^2}{2} \right) \\ & \left. + \frac{1}{3} \frac{2i}{(4f)^2} (2g_A^2 + \frac{1}{9} h_A^2) m^2 - \frac{m^2}{2} + O(Q^3) \right] : \quad (83) \end{aligned}$$

Here γ_6 plays a similar role to γ_1 for g_{NN} . The value of g_{NN} is complex because the intermediate pion and nucleon states for Fig. 10 (i) and (j) can go on shell.

V. RESULTS

As fixed input parameters, we use the standard baryon and pion masses: $M = 939 \text{ MeV}$, $M_\pi = 139 \text{ MeV}$, and $m_\pi = 139 \text{ MeV}$. We also take [41] $f_\pi = 92.4 \text{ MeV}$ from charged pion decay, $g_A = 1.26$ from neutron decay, and $h_A = 1.46$ from Eq. (63) with $g_N = h_A M = f_\pi$ and the central value of the width $\Gamma = 120 \text{ MeV}$. The physical results should be independent of the scale of dimensional regularization. To confirm that this is indeed the case we carry out calculations with three values of the scale, namely $\mu = M_\pi$, $\mu = 1 \text{ GeV}$, and $\mu = 0.75 \text{ GeV}$. We then have eleven free parameters left: a_0 , a_1 , a_2 , a_3 , a_4 , a_5 , a_6 , a_7 , a_8 , a_9 , and a_{10} . These are obtained by optimizing the fit of our calculated S- and P-wave phase shifts to the N scattering data of Amdt [42]. Because negligible error bars are given in the data at low energies, we assign all the data points the same relative weight in a least-squares fit. We fit the data for pion cm. kinetic energies between 10 and 100 MeV.

The fit obtained for the S- and P-wave phase shifts as a function of the pion cm. kinetic energy is indicated by the solid line in Fig. 12. Here the renormalization scale is chosen to be 1 GeV and the corresponding parameters are Set A1 in Table 1. The experimental data points of Amdt [42] to which we fit are displayed as triangles in Fig. 12; we also display there the older data of Bugg [45] (squares) and Koch and Pietarinen [46] (circles). The solid line shows a good fit up to 100 MeV pion cm. kinetic energy, slightly below the resonance at 127 MeV. It is remarkable that a good fit is achieved, even with eleven parameters, since the T-matrix contains a number of complicated non-polynomial functions of the invariant variables. The agreement for most of the phase shifts extends beyond 100 MeV, but δ_{31} starts to deviate markedly. Extending the range of cm. energies used for the fitting does not change the situation significantly. However, $O(Q^4)$ contributions may become significant above approximately 100 MeV. This assertion is supported by test calculations in which we have included a few selected contributions of this order. However, without considering all $O(Q^4)$ contributions no definitive statement can be made. A better strategy is to examine the renormalization scale dependence of the phase shifts. The dashed

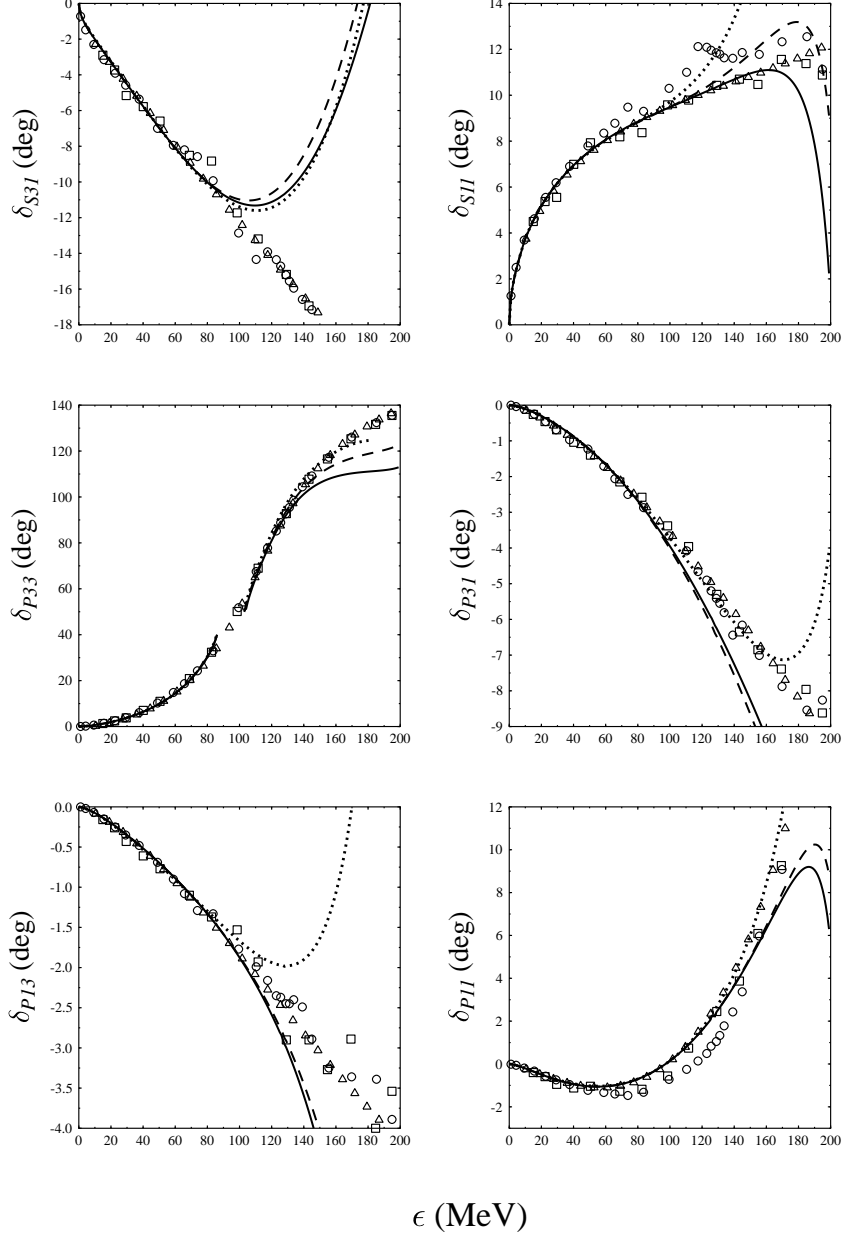


FIG. 12. The S- and P-wave phase shifts as a function of the pion cm. kinetic energy. The solid, dashed, and dotted curves are calculated with parameters sets A1 ($\epsilon = 1 \text{ GeV}$), A2 ($\epsilon = 1.232 \text{ GeV}$), and A3 ($\epsilon = 0.75 \text{ GeV}$) respectively. The data are from Amdt [42] (triangles), Bugg [45] (squares), and Koch and Pietarinen [46] (circles).

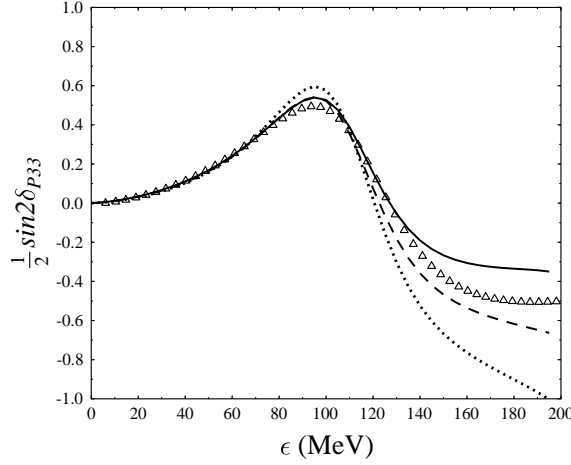


FIG. 13. The dependence of $\frac{1}{2} \sin 2 \delta_{P33}$ upon the pion c.m. kinetic energy. The phase-shift data from Amdt [42] are indicated by the triangles. The solid, dashed, and dotted curves are calculated with parameters sets A1, B1, and C1 respectively.

and dotted curves in Fig. 12 display results obtained with $\mu = M$ and $\mu = 0.75 \text{ GeV}$ respectively; the corresponding parameters are labelled Sets A2 and A3 in Table 1. The Q^2 values for the three different values of the scale are similar and the phase shifts agree up to 100 MeV. Beyond this energy a dependence on the scale starts to appear indicating that $O(Q^4)$ contributions are needed. The deviations are most noticeable for δ_{S31} and δ_{P13} which suggests that they are the most sensitive to higher-order contributions. We remark that similar results can be obtained with values of the renormalization scale as small as m_π . In Fig. 12 there is a small gap in the δ_{P33} phase shift just below 100 MeV. Here unitarity is slightly violated and a phase shift cannot be determined. The point is made in Fig. 13 where $\frac{1}{2} \sin 2 \delta_{P33}$ is plotted for Set A1 (solid curve). The maximum magnitude of $\frac{1}{2}$ is exceeded in a 10 MeV energy region by 10%. This is a small violation and the salient point is that sensible results are obtained without resorting to a phenomenological K -matrix approach to enforce unitarity.

While we expect the parameters of Table 1 to be natural, i.e. of order unity, some of them are close to 10. There could be several reasons for this. First, we have no definite prescription for assigning factors of 2 in the definition of the parameters. Second, the phase

shifts are derived from the T -matrix where there are strong cancellations among the various terms. This suggests that the parameters have significant uncertainties. Third, we note that the parameters are scale dependent. They appear more natural for Set A3 with $\Lambda = 0.75$ GeV than for Sets A1 and A2. An example of this is the parameter g_6 which contributes to the effective NN coupling, see Eq. (83). In fact the last row of the table shows that the effective NN couplings obtained from sets A1, A2, and A3 are quite similar and show a very small deviation from the tree-level value. Thus, we should not be unduly concerned by the size of some of the parameters.

In Table 1 we also show the value of the effective NN coupling, which remains close to the tree-level value. The NN coupling compares quite well with the determination of Amundt et al. [44] of $g_{NN} = (\frac{g_A M}{f}) = 1.03$. We also tabulate the nucleon sigma term calculated from Eq. (74). Essentially the same value is obtained for Sets A1, A2, and A3 so the sigma term is renormalization scale independent, as it should be. The magnitude of 108 MeV, however, is much larger than the generally accepted value of 45 ± 8 due to Gasser et al. [43]. It is only slightly reduced to 92 MeV when we fit to the older data of Koch and Pietarinen [46]. The value of $(2m^2)_{\pi\pi}(0) = 15.7$ MeV depends only on g and h_A and is uncontroversial [13,15,43]. Thus our predicted $(2m^2)_{\pi\pi}$ is also much larger than the value of 64 ± 8 MeV obtained [47] using dispersion relations. In order to see how sensitive our fit is to the sigma term, we make two other fits in which (0) is constrained to be 75 and 45 MeV respectively. This is achieved by fixing g_2 via Eq. (74), while allowing the remaining parameters to vary. We choose the scale of dimensional regularization to be $\Lambda = 1$ GeV. The parameters thus obtained are respectively labelled B1 and C1 in Table 1. The corresponding phase shifts are denoted by dashed and dotted lines in Fig. 14 and these can be compared with the solid curve obtained with Set A1. The value of a^2 for Set B1 is 50% larger than for Set A1 and only the s_{31} phase shift shows any visible difference between the two cases for c.m. energies below 100 MeV. The NN and N couplings are also similar. However, for set C1 a^2 is more than a factor of 2 greater than for Set A1 and larger differences appear for the phase shifts, particularly the S-waves, and couplings. Clearly (0) is not well determined,

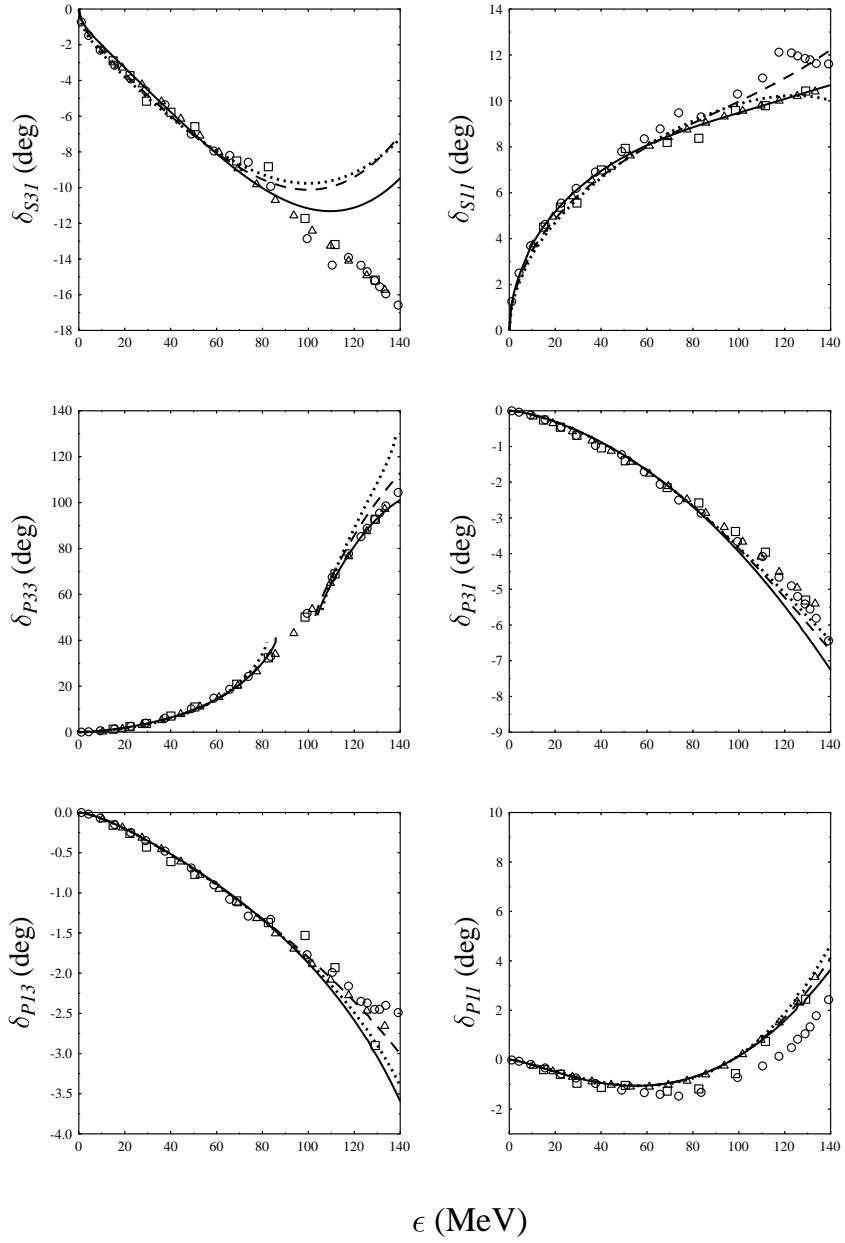


FIG. 14. The S- and P-wave phase shifts as a function of the pion cm. kinetic energy. The solid, dashed, and dotted curves are calculated with parameters sets A1, B1, and C1 respectively. The data are as in Fig. 12.

although values larger than 45 MeV are suggested. Note that Mojzis [16] obtained a value of 59 MeV by fitting to the threshold parameters, the NN coupling, and the sigma term. The parameters for Sets A1, B1, and C1 show some significant differences indicating, as mentioned earlier, that they are not well determined by fitting the phase shift data alone. We also note that Fig. 13 shows that Sets B1 and C1 violate unitarity at about 150 MeV cm^{-1} energy, although here, as we have remarked, we expect $O(Q^4)$ effects to be important. However, it may be significant that just below 100 MeV Set C1 gives a larger violation of unitarity than the other parameter sets.

It is also interesting to examine the threshold (vanishing pion kinetic energy) S-wave scattering lengths (a_{2I}) and the P-wave scattering volumes (a_{2I2J}). The experimental values were not used in the fit and they are compared with our predictions with Sets A1, B1, and C1 in Table II. The agreement for the P-waves is reasonable with not too much sensitivity to the parameter set, although a_{33} does become rather small for Set C1. For the S-waves it is instructive to examine the isoscalar and isovector scattering lengths, $b_0 = (a_1 + 2a_2)/3$ and $b_1 = (a_3 - a_1)/3$. For b_1 , Ref. [42], Ref. [46], and a recent determination by Sigg et al. [48] give 0.091 , 0.091 ± 0.002 and 0.096 ± 0.007 respectively. These are in agreement and somewhat larger in magnitude than our predicted value of 0.082 , virtually independent of parameter set. The value of b_0 from Ref. [42] is consistent with zero, while Refs. [46,48] give 0.010 ± 0.003 and 0.008 ± 0.007 . Our parameter sets A1, B1, and C1 give 0.003 , 0.013 , and 0.023 respectively. From this result, and the others that we have discussed, we conclude that parameter set C1 is less favored than the other sets. Note that we do not show the scattering lengths and volumes for Sets A2 and A3 because they differ negligibly from Set A1, indicating χ -independence. We make the obvious remark that the accuracy of the predicted scattering lengths and volumes can be improved by including them in the fit at the expense of a poorer fit to the phase shifts. In the case of Set A this reduces the sigma term by about 10%.

VI. CONCLUSIONS

We have introduced a new approach to chiral perturbation theory with baryons which involves manipulating the Feynman diagrams directly, rather than integrating out the heavy components of the baryon fields at the Lagrangian level as in HB χ PT. Our approach preserves Weinberg's power counting so that a systematic expansion in powers of a generic soft momentum scale, Q , remains valid. We can maintain relativistic covariance and apply the standard Feynman rules and matrix algebra. At one-loop order we obtain equivalent results to HB χ PT; it would be interesting to compare the approaches in higher order.

We have calculated the T -matrix for NN scattering up to one-loop Q^3 order. There were several components to this calculation. First, the chiral Lagrangian introduced a number of contact terms with unknown coefficients which contributed to the T -matrix. Next, there were the well-known nucleon and Δ exchange diagrams. The former was straightforward, but the latter was singular at tree level when the Δ went on shell. The problem was solved by summing up $O(Q^3)$ self-energy insertions in the propagator to all orders. The resulting amplitude then (approximately) obeyed unitarity for pion c.m. energies up to at least 140 MeV. Finally, we needed to evaluate the large number of one-loop diagrams which could be constructed with the π , N and Δ vertices.

We have performed a least-squares fit to the S - and P -wave phase shift data to determine the parameters involved. We were able to obtain a good fit up to 100 MeV pion c.m. kinetic energy, slightly below the Δ resonance. Our predictions for the zero-energy scattering lengths were also reasonable. These results were independent of the renormalization scale, μ , as they should be. Since πN is an expansion parameter and at the Δ resonance it becomes $\pi N = 0.27$, one might expect $O(Q^4)$ effects to become important beyond the resonance energy. This was supported by the scale dependence of our results in that energy region. Though straightforward in principle, it would be very tedious to include the $O(Q^4)$ corrections. The fit that we have obtained here contained an unavoidably large number of parameters, but it must be borne in mind that the T -matrix is a much more complicated

function of the invariant variables when loops are present than at tree level. Thus we regard the fit that we have achieved as a vindication of the basic approach. It seems, however, that one cannot determine the parameters with great accuracy using the phase shift data alone. In particular we were able to obtain very similar fits with parameters that corresponded to a nucleon mass of 105 and 75 MeV. We judge that the fit was slightly degraded when the currently accepted value of $m(0) = 45 \text{ MeV}$ was adopted, so that a somewhat larger value appears to be favored from the analysis here. However this might indicate that $O(Q^4)$ effects need to be calculated in order to achieve an accurate one-loop result, as Ecker has recently argued [49]. It would be interesting to attempt to constrain the parameters further and to compare with the parameters found at zero energy [15,16]. The latter would involve disentangling the contributions as well as other effects that, for simplicity, we have absorbed in the contact terms.

We thank S. Jeon and J. Kapusta for useful discussions and critical readings of the manuscript. We acknowledge support from the Department of Energy under grant No. DE-FG 02-87ER 40328.

APPENDIX :

We first list the integrals we need. Using dimensional regularization we obtain

$$i^{-4} \int \frac{d^d k}{(2\pi)^d} \frac{1}{(k^2 - m^2 + i\epsilon)[(k+Q)^2 - m^2 + i\epsilon]} = 2L - \frac{1}{(4\pi)^2} I(Q^2); \quad (\text{A } 1)$$

where L , defined in Eq. (35), is singular and the finite part

$$I(x) = 1 - \ln \frac{m^2}{2} - \frac{s}{1 - \frac{4m^2}{x}} \ln \frac{1 - \frac{4m^2}{x} + 1}{1 - \frac{4m^2}{x}} \quad \text{for } x < 0; \quad (\text{A } 2)$$

The next integral to consider is

$$i^{-4} \int \frac{d^d k}{(2\pi)^d} \frac{1}{(k^2 - m^2 + i\epsilon)(2p \cdot k + z + i\epsilon)} = \frac{z}{p^2} L - \frac{1}{(4\pi)^2} \frac{1}{p^2} \frac{z}{p^2} \frac{1}{2} \frac{z}{p^2} \frac{1}{p^2} \frac{1}{16 p^2} \frac{i}{(z)^2} \frac{(z^2 - 4p^2 m^2)}{4p^2 m^2} \frac{1}{z^2 - 4p^2 m^2}; \quad (\text{A } 3)$$

where θ denotes the Heaviside step function and

$$J(x) = \begin{cases} \frac{1}{2} \ln \frac{x^2 - m^2}{x^2 + m^2} & (x > m) \\ \frac{1}{2} \ln \frac{x^2 + m^2}{x^2 - m^2} & (x < m) \end{cases} \quad (A4)$$

Note that $J(0) = \frac{1}{2} \ln \frac{m^2}{m^2} = 0$. The next integral we need is finite:

$$i^4 \int_0^{\infty} \frac{d^4 \lambda}{(2\pi)^4} \frac{1}{(\lambda^2 - m^2 + i\epsilon)[(\lambda + Q)^2 - m^2 + i\epsilon](2p - \lambda + i\epsilon)} = \frac{1}{16} \frac{1}{p^2(4m^2 - Q^2)} S(Q^2); \quad (A5)$$

where

$$S(x) = \begin{cases} \frac{1}{x} \sin^{-1} \frac{1}{1 - \frac{4m^2}{x}} & \text{for } x < 0 \end{cases} \quad (A6)$$

Finally we require the finite integral

$$i^4 \int_0^{\infty} \frac{d^4 \lambda}{(2\pi)^4} \frac{1}{(\lambda^2 - m^2 + i\epsilon)[(\lambda + Q)^2 - m^2 + i\epsilon](2p - \lambda + i\epsilon)} = \frac{1}{32\pi^2 M} \int_0^1 dx K(x); \quad (A7)$$

where

$$K(x) = \begin{cases} \frac{1}{2} \ln \frac{x^2 - m^2 + x(1-x)Q^2}{x^2 - m^2 + x(1-x)Q^2} & (x^2 - m^2 + x(1-x)Q^2 > 0) \\ \frac{1}{2} \tan^{-1} \frac{x(1-x)Q^2}{x^2 - m^2 + x(1-x)Q^2} & (x^2 - m^2 + x(1-x)Q^2 < 0) \end{cases} \quad (A8)$$

In Ref. [16] the expressions for the integrals of Eqs. (A1), (A3), and (A5) are written in terms of $J_0(Q^2)$,

$J_0(z) = \frac{1}{4p^2} \ln \frac{z + 4p^2}{z - 4p^2}$, and $K_0(0; Q^2) = \frac{1}{4p^2}$; they agree with our results above. Our expressions are written in terms of M , μ , and λ and we recall the definitions for reference

$$M = \frac{1}{2}(M_1 + M_2); \quad \mu = M_1 - M_2; \quad \lambda = \frac{s}{2M} \quad (A9)$$

It is useful to define the functions

$$F_1(\mu; \lambda) = \frac{1}{(\lambda^2 - \mu^2)^2} \left[(2\lambda^2 - \mu^2)J(\lambda) + (2\lambda^2 - 3\mu^2 + m^2)J(\mu) \right] + (\lambda^2 - \mu^2)^2 \ln \frac{m^2}{2} \quad (A10)$$

$$F_2(\mathbf{k}; \mathbf{k}') = \frac{1}{(4\pi f)^2} \left(\frac{h}{2} m^2 J(\mathbf{k}) - \frac{h}{2} m^2 J(\mathbf{k}') + m^3 \left(\frac{h}{2} \right) \right) \quad (\text{A } 11)$$

$$F_3(\mathbf{k}; \mathbf{k}') = \frac{1}{(4\pi f)^2} \left(\frac{h}{2} m^2 J(\mathbf{k}) - \frac{h}{2} m^2 J(\mathbf{k}') + \frac{1}{2} m^2 \left(\frac{h}{2} \right) \ln \frac{m^2}{2} \right) : \quad (\text{A } 12)$$

These functions are finite, for example,

$$F_3(\mathbf{k}; \mathbf{k}') = \frac{1}{(4\pi f)^2} \left(\frac{h}{2} m^2 J(\mathbf{k}) - \frac{h}{2} m^2 J(\mathbf{k}') + \frac{3}{2} m^2 \ln \frac{m^2}{2} \right) : \quad (\text{A } 13)$$

Then the contributions from Figs. 9 and 10 to the real part of the T-matrix for N scattering are:

$$T_{9a}^+ = \frac{g_A^2}{12f^2} \frac{1}{(4\pi f)^2} \left((4m^2 - 12t)m + \frac{3(m^2 - 2t)(2m^2 - t)}{4m^2 - t} S(t) \right) ; \quad (\text{A } 14)$$

$$T_{9a} = \frac{g_A^2}{12f^2} \frac{1}{(4\pi f)^2} \left((8m^2 - 5t)I(t) + 10 m^2 \ln \frac{m^2}{2} \right. \\ \left. + \frac{h}{6} M \not{q} M + \frac{1}{4} (2m^2 - t) \frac{ih}{2m} + \frac{q}{4m^2 - t} S(t) \right) ; \quad (\text{A } 15)$$

$$T_{9b}^+ = \frac{2h_A^2}{9f^2} \frac{1}{(4\pi f)^2} \left(\frac{4}{3} (7m^2 - 6t - 4^2) J(\mathbf{k}) + 2 (m^2 - 2t) I(t) \right. \\ \left. + (m^2 - 2t) (2^2 - 2m^2 + t) \int_0^{\frac{1}{2}} dx K(x) - \frac{8}{3} m^2 \ln \frac{m^2}{2} \right) ; \quad (\text{A } 16)$$

$$T_{9b} = \frac{4h_A^2}{9f^2} \frac{1}{(4\pi f)^2} \left(\frac{h}{6} M \not{q} M + \frac{1}{4} (2m^2 - t) + 4 \frac{h}{2} J(\mathbf{k}) \right. \\ \left. + \frac{h}{6} M \not{q} M + \frac{1}{4} (2m^2 - t) + 2^2 - \frac{4}{3} m^2 + \frac{5}{6} t I(t) \right. \\ \left. + \frac{h}{6} M \not{q} M + \frac{1}{4} (2m^2 - t) \right. \\ \left. + 2^2 - m^2 + \frac{1}{2} t \int_0^{\frac{1}{2}} dx K(x) + \frac{5}{3} m^2 \ln \frac{m^2}{2} \right) ; \quad (\text{A } 17)$$

$$T_{9c}^{ba} = \frac{1}{2} [\mathbf{b}; \mathbf{a}] \frac{1}{12f^2} \frac{1}{(4\pi f)^2} (4m^2 - t) I(t) - 2m^2 \ln \frac{m^2}{2} ; \quad (\text{A } 18)$$

$$T_{9d}^{ba} = \mathbf{ab} + \frac{1}{4} [\mathbf{b}; \mathbf{a}] \frac{1}{f^2} \frac{1}{(4\pi f)^2} J(\mathbf{k}) + \frac{3}{8} m^2 \ln \frac{m^2}{2} ; \quad (\text{A } 19)$$

$$T_{9e}^{ba} = \mathbf{ab} - \frac{1}{6} [\mathbf{b}; \mathbf{a}] \frac{g_A^4}{4f^2} \frac{1}{(4\pi f)^2} M \not{q} M + 2m^2 - t - \frac{3}{2} 2^2 F_1(\mathbf{k}; 0) ; \quad (\text{A } 20)$$

$$T_{9f}^{ba} = \mathbf{ab} + \frac{1}{12} [\mathbf{b}; \mathbf{a}] \frac{2g_A^2}{9f^2} \frac{h_A^2}{(4\pi f)^2} F_1(\mathbf{k}; 0) \\ + \frac{h}{6} M \not{q} M - \frac{5}{4} (2m^2 - t) + 3^2 \frac{h}{2} ; \quad (\text{A } 21)$$

$$T_{9g}^{ba} = T_{9h}^{ba} = \frac{1}{2} [{}^b; {}^a] \frac{4g_A^2}{27f^2} \frac{h_A^2}{(4-f)^2} M \not{M} + \frac{1}{4} (2m^2 - t) F_2 \left(\frac{t}{4-f}; \frac{t}{4-f} \right); \quad (\text{A } 22)$$

$$T_{9i}^{ba} = T_{9j}^{ba} = \frac{1}{2} [{}^b; {}^a] \frac{20h_A^2}{243f^2} \frac{g_A \tilde{h}_A}{(4-f)^2} M \not{M} + \frac{1}{4} (2m^2 - t) F_2 \left(\frac{t}{4-f}; \frac{t}{4-f} \right); \quad (\text{A } 23)$$

$$T_{9k}^{ba} = {}^{ab} + \frac{5}{12} [{}^b; {}^a] \frac{40h_A^4}{81f^2} \frac{1}{(4-f)^2} F_1 \left(\frac{t}{4-f}; \frac{t}{4-f} \right) \\ M \not{M} + \frac{1}{20} (2m^2 - t - 12^2) \frac{t}{4-f}; \quad (\text{A } 24)$$

$$T_{9l}^{ba} = {}^{ab} + \frac{1}{6} [{}^b; {}^a] \frac{100h_A^2}{729f^2} \frac{\tilde{h}_A^2}{(4-f)^2} F_1 \left(\frac{t}{4-f}; \frac{t}{4-f} \right) \\ M \not{M} + \frac{1}{2} (2m^2 - t - 3^2) \frac{t}{4-f}; \quad (\text{A } 25)$$

$$T_{9m}^{ba} = {}^{ab} + \frac{1}{2} [{}^b; {}^a] \frac{3g_A^4}{4f^2} \frac{1}{(4-f)^2} M \not{M} + \frac{1}{2} {}^2 F_1 \left(\frac{t}{4-f}; 0 \right); \quad (\text{A } 26)$$

$$T_{9n}^{ba} = {}^{ab} + \frac{1}{2} [{}^b; {}^a] \frac{4g_A^2}{3f^2} \frac{h_A^2}{(4-f)^2} M \not{M} + \frac{1}{2} {}^2 F_1 \left(\frac{t}{4-f}; \frac{t}{4-f} \right); \quad (\text{A } 27)$$

$$T_{9o}^{ba} = \frac{1}{2} [{}^b; {}^a] \frac{5}{24f^2} \frac{1}{(4-f)^2} m^2 \ln \frac{m^2}{2}; \quad (\text{A } 28)$$

$$T_{9p}^{ba} = \frac{1}{2} [{}^b; {}^a] \frac{g_A^2}{8f^2} \frac{1}{(4-f)^2} m^2 \left(2 + 3 \ln \frac{m^2}{2} \right); \quad (\text{A } 29)$$

$$T_{9q}^{ba} = \frac{1}{2} [{}^b; {}^a] \frac{20h_A^2}{9f^2} \frac{1}{(4-f)^2} m^2 \left(2^2 + 3 J \left(\frac{t}{4-f} \right) + \frac{3}{2} m^2 \ln \frac{m^2}{2} \right); \quad (\text{A } 30)$$

$$T_{9r}^{ba} = T_{9s}^{ba} = {}^{ab} \frac{g_A^2}{3f^2} \frac{m^3}{(4-f)^2}; \quad (\text{A } 31)$$

$$T_{9t}^{ba} = T_{9u}^{ba} = {}^{ab} \frac{16h_A^2}{27f^2} \frac{1}{(4-f)^2} \left({}^2 m^2 \right) J \left(\frac{t}{4-f} \right) + \frac{1}{2} m^2 \ln \frac{m^2}{2}; \quad (\text{A } 32)$$

$$T_{10a}^{ba} = {}^{ab} + \frac{1}{2} [{}^b; {}^a] \frac{2g_A}{M^2 f^2} M \not{M}; \quad (\text{A } 33)$$

$$T_{10b}^{ba} = {}^{ab} + \frac{1}{2} [{}^b; {}^a] \frac{g_A^2}{3f^2} \frac{1}{(4-f)^2} M \not{M} + \frac{1}{2} {}^2 \frac{m^2}{4-f} \ln \frac{m^2}{2}; \quad (\text{A } 34)$$

$$T_{10c}^{ba} = {}^{ab} + \frac{1}{2} [{}^b; {}^a] \frac{g_A^4}{6f^2} \frac{1}{(4-f)^2} M \not{M} + \frac{1}{2} {}^2 F_3 \left(\frac{t}{4-f}; 0 \right); \quad (\text{A } 35)$$

$$T_{10d}^{ba} = {}^{ab} + \frac{1}{2} [{}^b; {}^a] \frac{32g_A^2}{27f^2} \frac{h_A^2}{(4-f)^2} M \not{M} + \frac{1}{2} {}^2 F_3 \left(\frac{t}{4-f}; \frac{t}{4-f} \right); \quad (\text{A } 36)$$

$$T_{10e}^{ba} = {}^{ab} + \frac{1}{2} [{}^b; {}^a] \frac{32g_A^2}{27f^2} \frac{h_A^2}{(4-f)^2} M \not{M} + \frac{1}{2} {}^2 F_3 \left(\frac{t}{4-f}; 0 \right); \quad (\text{A } 37)$$

$$T_{10f}^{ba} = \quad ab + \frac{1}{2} [\quad b; \quad a] \quad \frac{200h_A^2}{243f^2} \frac{g_A \tilde{h}_A}{(4-f)^2} M \not{q} \quad M + \frac{1}{2} \quad^2 F_3 (\quad ; \quad) ; \quad (A 38)$$

$$T_{10g}^{ba} = \quad ab \quad \frac{1}{4} [\quad b; \quad a] \quad \frac{8h_A}{3f^2} \frac{m^2}{M^2} [\quad_1(s;t) + \quad_2(s;t)\not{q}] \quad_R(s) ; \quad (A 39)$$

$$T_{10h}^{ba} = \quad ab \quad \frac{1}{4} [\quad b; \quad a] \quad \frac{4h_A^2}{9f^2} \frac{1}{(4-f)^2} m^2 \ln \frac{m^2}{2} \quad_1(s;t) + \quad_2(s;t)\not{q}^i \quad_R(s) ; \quad (A 40)$$

$$T_{10i}^{ba} = \quad ab \quad \frac{1}{4} [\quad b; \quad a] \quad \frac{8g_A^2}{9f^2} \frac{h_A^2}{(4-f)^2} \quad_1(s;t) + \quad_2(s;t)\not{q}^i \quad F_3 (\quad ; 0) \quad_R(s) + \frac{12 \quad^2 f^2}{h_A^2} \frac{M \quad^2 (s)}{[s - M^2 (\quad)]^2 + M^2 \quad^2 (s)} ; \quad (A 41)$$

$$T_{10j}^{ba} = \quad ab \quad \frac{1}{4} [\quad b; \quad a] \quad \frac{8h_A^4}{81f^2} \frac{1}{(4-f)^2} \quad_1(s;t) + \quad_2(s;t)\not{q}^i \quad F_3 (\quad ; \quad) \quad_R(s) + \frac{12 \quad^2 f^2}{h_A^2 (\quad + \quad)} \frac{M \quad^2 (s)}{[s - M^2 (\quad)]^2 + M^2 \quad^2 (s)} ; \quad (A 42)$$

$$T_{10k}^{ba} = \quad ab \quad \frac{1}{4} [\quad b; \quad a] \quad \frac{50h_A^2}{81f^2} \frac{g_A \tilde{h}_A}{(4-f)^2} \quad_1(s;t) + \quad_2(s;t)\not{q}^i F_3 (\quad ; 0) \quad_R(s) ; \quad (A 43)$$

$$T_{10l}^{ba} = \quad ab \quad \frac{1}{4} [\quad b; \quad a] \quad \frac{200 h_A^2}{729 f^2} \frac{\tilde{h}_A^2}{(4-f)^2} \quad_1(s;t) + \quad_2(s;t)\not{q}^i F_3 (\quad ; \quad) \quad_R(s) : \quad (A 44)$$

Notice Eqs. (A 33) { (A 36) for diagrams 10 (g){10 (l) have been written in terms of $\quad_1; \quad_2$ of Eq. (66) rather than truncating these expressions to $O(\quad^2)$. This is necessary to ensure that the resonance only contributes to the P_{33} channel and does not "contaminate" the other channels. To the above contributions should be added the results for the cross diagrams where applicable. They are obtained from the listed expressions by the replacements $\quad \rightarrow \quad$, $(u - \hat{M}) = (2M - \quad)$, and the interchanges $a \leftrightarrow b$ and $q \leftrightarrow \not{q}$.

REFERENCES

- [1] M . G . O l s s o n and E . T . O s y p o w s k i, Nucl. Phys. B 101, 136 (1975).
- [2] D . B o n g e r and W . S . W o o l c o c k, Nuovo C i m . A 104, 1489 (1991).
- [3] B . C . P e a r c e and B . K . J e n n i n g s, Nucl. Phys. A 528, 655 (1991).
- [4] F . G r o s s and Y . S u r y a, Phys. Rev. C 47, 703 (1993).
- [5] P . F . A . G o u d s m i t, H . J . L e i s i, E . M a t s i n o s, B . L . B i r b r a i r and A . B . G r i d n e v, Nucl. Phys. A 575, 673 (1994).
- [6] P . J . E l l i s and H . B . T a n g, Phys. Rev. C 56, 3363 (1997).
- [7] S . W e i n b e r g, Physica A 96, 327 (1979).
- [8] J . G a s s e r and H . L e u t w y l e r, Ann. Phys. 158, 142 (1984); Nucl. Phys. B 250, 465, 517, 539 (1985).
- [9] J . G a s s e r, M . E . S a i n i o, and A . S v a r c, Nucl. Phys. B 307, 779 (1988).
- [10] E . J e n k i n s and A . V . M a n o h a r, Phys. Lett. B 255, 558 (1991).
- [11] H . B . T a n g, hep-ph/9607436.
- [12] R . D . P e c c e i, Phys. Rev. 176, 1812 (1963).
- [13] V . B e m a r d, N . K a i s e r and U l f G . M e i n e r, Int. J. Mod. Phys. E 4, 193 (1995).
- [14] V . B e m a r d, N . K a i s e r and U l f G . M e i n e r, Phys. Rev. C 52, 2185 (1995).
- [15] V . B e m a r d, N . K a i s e r and U l f G . M e i n e r, Nucl. Phys. A 615, 483 (1997).
- [16] M . M o j z i s, Eur. Phys. J. C 2, 181 (1998).
- [17] A . D a t t a and S . P a k v a s a, Phys. Rev. D 56, 4322 (1997).
- [18] C . C a l l a n, S . C o l e m a n, J . W e s s and B . Z u m i n o, Phys. Rev. 177, 2247 (1969).

- [19] R. J. Fumstahl, H.-B. Tang, and B. D. Serot, Nucl. Phys. A 615, 441 (1997).
- [20] S. Weinberg, Phys. Lett. B 251, 288 (1990); Nucl. Phys. B 363, 3 (1991).
- [21] A. Krause, Helvetica Phys. Acta 63, 3 (1990).
- [22] L. M. Nath, B. Etemadi and J. D. Kimel, Phys. Rev. D 3, 2153 (1970).
- [23] H.-B. Tang and P. J. Ellis, Phys. Lett. B 387, 9 (1996).
- [24] H. Georgi, Phys. Lett. B 298, 187 (1993).
- [25] H. Georgi, Nucl. Phys. B 361, 339 (1991).
- [26] C. Arzt, Phys. Lett. B 342, 189 (1995).
- [27] J. Gasser, Workshop on Chiral Dynamics (Mainz, 1997), hep-ph/9711503.
- [28] A. V. Manohar and H. Georgi, Nucl. Phys. B 234, 189 (1984).
- [29] G. P. Lepage, in From Actions to Answers (TASI-89), ed. T. DeGrand and D. Toussaint (World Scientific, Singapore, 1989) p. 483.
- [30] J. C. Collins, Renormalization (Cambridge University Press, 1984).
- [31] V. Bernard, N. Kaiser, J. Kambor, and U. G. Meißner, Nucl. Phys. B 388, 315 (1992).
- [32] T. R. Hemmert, B. R. Holstein and J. Kambor, Phys. Lett. B 395, 89 (1997).
- [33] G. Hohler, Pion-Nucleon Scattering, Landolt-Bornstein, New Series, ed. H. Schopper, Vol. I/9 b2 (Springer-Verlag, Berlin, 1983).
- [34] T. Ericson and W. Weise, Pions and Nuclei (Oxford University Press, 1988).
- [35] P. Van Nieuwenhuizen, Phys. Rep. 68, 189 (1981).
- [36] M. Benmerrouche, R. M. Davidson and N. C. Mukhopadhyay, Phys. Rev. C 39, 2339 (1989).

- [37] S. Gasiorowicz, Elementary Particle Physics (John Wiley & Sons, NY, 1966).
- [38] L. S. Brown, W. J. Pardee and R. D. Peccei, Phys. Rev. D 4, 2801 (1971).
- [39] V. Bernard, N. Kaiser and Ulf-G. Meißner, Phys. Lett. B 389, 144 (1996).
- [40] T. P. Cheng and L. F. Li, Gauge Theory of Elementary Particle Physics (Oxford University Press, 1984)
- [41] Particle Data Group, R. M. Barnett et al., Phys. Rev. D 54, 1 (1996).
- [42] R. A. Amdt, SAID dial-in program using data le PN 961fPIN data VP I&SU, 2/26/96.
- [43] J. Gasser, H. Leutwyler and M. E. Sainio, Phys. Lett. B 253, 252 (1991).
- [44] R. A. Amdt, R. L. Workman, and M. M. Pavan, Phys. Rev. C 49, 2729 (1994).
- [45] D. V. Bugg, Int. Symp. on Pion-Nucleon Physics and the Structure of the Nucleon (Bad Honnef, Germany, 1991), ed. R. Decker, G. Hohler, M. G. Huber and W. Kluge, Newsletter 6, 7 (1992).
- [46] R. Koch and E. Pietarinen, Nucl. Phys. A 336, 331 (1980).
- [47] R. Koch, Z. Phys. C 15, 161 (1982).
- [48] D. Sigg, A. Badertscher, M. Bogdan, P. F. A. Goudsmidt, H. J. Leisi, H.-Ch. Schroder, Z. G. Zhao, D. Chatellard, J.-P. Egger, E. Jeannet, E. C. Aschenauer, K. Gabathuler, L. M. Simons, and A. J. RusiElHasani, Nucl. Phys. A 609, 269 (1996); (E) A 617, 526 (1997).
- [49] G. Ecker, Workshop on Chiral Dynamics (Mainz, 1997), hep-ph/9710560.

TABLE I. Parameter sets obtained from fitting the N phase shifts for various values of the renormalization scale μ . The deduced NN and N couplings and the nucleon term are also given.

	A 1	A 2	A 3	B 1	C 1
(GeV)	1.00	1.232	0.75	1.00	1.00
	3.5790	4.2084	1.9714	3.1385	3.1641
	2.3219	3.5370	0.1993	1.9697	2.3169
1	5.6578	6.5464	1.5485	4.6914	5.2765
2	2.3683	2.5845	2.1417	1.9931 ^y	1.6286 ^y
1	2.6652	1.9338	4.2176	2.2593	9.7605
2	6.4822	4.5533	7.7712	8.2178	11.7498
3	11.0504	11.9228	4.6877	10.7125	15.2134
4	4.4304	2.5495	6.3775	6.1955	9.6040
5	4.9702	3.5669	4.1456	5.3523	8.0874
6	9.3759	9.2927	4.8363	7.3192	7.4099
\tilde{h}_A	1.6243	1.4418	1.0986	1.6779	2.4626
μ (MeV)	106	109	108	75	45
$g_{NN} = (\frac{g_A M}{f})$	1.0445	1.0378	1.0409	1.0091	0.9585
$\tilde{g}_N = \tilde{f}(\frac{h_A M}{f})$	0.9898	1.0134	1.0337	1.0532	1.1294

^y Fixed so as to obtain the listed value of μ (0).

TABLE II. The calculated S-wave scattering lengths and P-wave scattering volumes, in units of m^{-1} and m^{-3} respectively, are compared with the data of Refs. [42] and [46].

length/volume	A 1	B 1	C 1	Ref. [42]	Ref. [46]
a_1	0.168	0.152	0.142	0.175	0.173 0.003
a_3	0.080	0.095	0.105	0.087	0.101 0.004
a_{11}	0.078	0.075	0.070	0.068	0.081 0.002
a_{13}	0.026	0.026	0.025	0.022	0.030 0.002
a_{31}	0.035	0.036	0.035	0.039	0.045 0.002
a_{33}	0.201	0.188	0.171	0.209	0.214 0.002